ADVANCED FUNCTIONAL MATERIALS
www.afm-journal.de

Synchrotron Radiation for Quantum Technology

Oliver Rader, Sakura Pascarelli, Klaus Attenkofer, Anna A. Makarova, Karsten Holldack, Kai Rossnagel, Kristiaan Temst, George Kourousias, Stefano Carretta, Caterina Biscari, and Helmut Dosch*

In recent years, quantum technology has undergone transformative advancements, opening up unprecedented possibilities in computation, metrology, sensing, and communication and reshaping the landscape of scientific research. Based on superposition, interference, and entanglement of quantum states, quantum systems leverage the core principles of quantum mechanics to achieve performances that were once deemed impossible or computationally insurmountable by classical methods. However, the practical realization of devices hinges on the conservation of these quantum states and their precise manipulation, requiring materials engineering with atomic precision on many length scales —a formidable challenge. Synchrotron light and free-electron laser (FEL) facilities, widely employed across diverse scientific and engineering disciplines, provide important single techniques and suites of multimodal non-destructive imaging and diagnostic tools to reveal electronic, structural, and morphological properties of matter on device level. This article delves into how these tools can help to unlock the potential of quantum device technologies, overcoming production barriers and paving the way for future breakthroughs. Moreover, the article presents quantum optics in the x-ray regime using synchrotron and FEL light sources and addresses the potential of quantum computing for synchrotron-radiation experiments.

1. Introduction

Quantum technology, the realm where quantum mechanics merges with engineering, has rapidly emerged as a promising frontier in scientific research and technological innovation. Quantum systems, which harness the counterintuitive phenomena exhibited at the quantum scale, hold tremendous potential for revolutionizing numerous fields, including computation, cryptography, communication, and sensing. These systems exploit the principles of superposition, interference and entanglement to perform computations more efficiently, secure communication channels, and achieve unprecedented levels of precision in measurement.

However, the realization of practical quantum technologies faces numerous challenges. Quantum systems are inherently delicate and susceptible to environmental perturbations, making their precise control and manipulation highly challenging. Additionally, the

O. Rader, A. A. Makarova, K. Holldack
Helmholtz-Zentrum Berlin für Materialien und Energie
Albert-Einstein-Straße 15, 12489 Berlin, Germany
E-mail: rader@helmholtz-berlin.de

S. Pascarelli
European XFEL
Holzkoppel 4, 22869 Schenefeld, Germany

K. Attenkofer, C. Biscari
ALBA Synchrotron
Carrer de la Llum 2-26, Cerdanyola del Vallès, Barcelona 08290, Spain

K. Rossnagel
Institut für Experimentelle und Angewandte Physik
Christian-Albrechts-Universität zu Kiel
24118 Kiel, Germany

The ORCID identification number(s) for the author(s) of this article can be found under https://doi.org/10.1002/adfm.202501043

DOI: 10.1002/adfm.202501043

K. Rossnagel
Ruprecht Haensel Laboratory
Deutsches Elektronen-Synchrotron DESY
Notkestraße 85, 22607 Hamburg, Germany

K. Temst
Quantum Solid State Physics, KU Leuven
Celestijnenlaan 200 D, 3001 Leuven and imec, Kapeldreef 75, Leuven 3001, Belgium

G. Kourousias
Elettra - Sincrotrone Trieste
Strada Statale 14 - km 163.5 in AREA Science Park, Trieste, Basovizza 34149, Italy

S. Carretta
Dipartimento di Scienze Matematiche, Fisiche e Informatiche
Università di Parma
Parma 43124, Italy

S. Carretta
INFN – Sezione di Milano-Bicocca
Gruppo Collegato di Parma
Parma 43124, Italy

H. Dosch
Deutsches Elektronen-Synchrotron DESY
Notkestraße 85, 22607 Hamburg, Germany

characterization and measurement of quantum systems and devices with high fidelity are essential for understanding their behavior, optimizing their performance, and identifying sources of error.

This leads to the importance of materials science for quantum technology. Materials science for quantum computing hardware has been reviewed by de Leon et al.[1] and by Lordi and Nichol in a special issue[2] and for superconducting qubits by Murray.[3] In addition, quantum materials are becoming increasingly more important for the development of quantum technologies. The term refers to those materials exhibiting phenomena such as superconductivity, strong electron correlations, nontrivial topology, and pronounced proximity effects, and often involves an entanglement of charge, spin, orbital, and lattice degrees of freedom. Reviews of layered quantum materials for quantum technology have appeared[4,5] with a focus on light-matter interfaces as application area.[5]

Accelerator-based photon sources emerge as powerful analytical tools for scientists working in the field of quantum technology. Synchrotron radiation is the electromagnetic radiation emitted by charged particles held at or accelerated to relativistic speeds in storage rings and linear accelerators, respectively. These sources generate intense beams of light spanning a wide range of wavelengths, from infrared to X-rays, with exceptional brilliance where brilliance is the photon flux normalized by the solid angle of the emission, the source size, and a specific energy band. Other properties of synchrotron radiation are polarization, coherence, tunability, and time structure. Synchrotron radiation has been extensively utilized in atomic physics, materials science, and various other scientific disciplines, but its potential in advancing quantum technology has only recently begun to be explored.

In the following sections, we will delve into the specific applications of synchrotron radiation in quantum technology. We will discuss its use in characterizing conventional and quantum materials, where they are relevant for quantum technology, and optimizing device performance, where we distinguish electronic and optical quantum devices. In addition, we address the extension of quantum optics into the X-ray range and the impact of quantum computing on accelerators and synchrotron-radiation experiments. We will explore recent experimental achievements and present potential future directions for a fruitful collaboration between the application of synchrotron radiation and quantum technology, in particular toward exploiting European synergies. The significant allocation of public funds to bolster quantum technology research in Europe has led to the formulation of a cohesive strategy outlined in a technology roadmap.[6] Likewise, LEAPS, the League of European Accelerator-based Photon Sources, aims at pooling expertise and resources by increased collaboration towards technological challenges, including quantum technology.[7,8]

G. Kourousias
Department of Engineering and Architecture
University of Trieste
Piazzale Europa 1, Trieste 34127, Italy

2. Synchrotron Radiation Methods and Quantum Technologies

2.1. Overview of Synchrotron Radiation Methods

Since the discovery of synchrotron radiation emitted by relativistic electrons in 1947, many dedicated synchrotron radiation facilities and free electron lasers (FELs) have been developed over the past almost 80 years and more than 50 are operational today. This is due to the special properties of synchrotron radiation, which is emitted by accelerator-based sources over the entire spectral range from the far infrared (THz) to very hard X-ray photons up to 100 keV and beyond. The enormous brilliance, photon density (flux), tunability and coherence properties as well as the special time structure of these sources are still unique in the X-ray range and render these sources a versatile tool for material analysis and in particular to study quantum materials on various length (down to few nm) and time scales (even attoseconds).

Depending on the scientific question, one can exploit the fact that electrons, ions or photons are emitted during the interaction of X-rays with matter. The X-rays themselves are scattered, diffracted or generate fluorescence radiation. From this, a variety of synchrotron radiation methods have emerged as indispensable probes for the atomic and electronic structure of quantum materials at the surface and in the bulk. The potential of these methods and their new opportunities at 4th generation sources (i.e., those that are designed to achieve significantly higher brilliance and coherence, namely diffraction-limited storage rings and high-repetition FELs) are described in more detail below, together with their links to quantum technology as illustrated in **Figure 1** showing applications, challenges, and solutions.

2.2. Imaging and Diffraction

Synchrotron radiation, and in particular X-rays at short wavelengths, is capable of analyzing the micro and even nanostructure, the static and dynamic properties as well as the functionality of electronic devices through imaging and spectroscopy and the combination of the two. Imaging may be performed in 2D or 3D with contrast achieved either through spectroscopic or diffraction methods. The deep penetration of hard X-rays enables studies of buried interfaces, especially at higher photon energies > 10 keV, and allows in situ analysis of thin film growth. Soft- (< 2 keV) and tender X-rays (< 5 keV) require vacuum and absence of windows. With the increased coherence of 4th generation synchrotron radiation sources, it is easier to recover the phase information in X-ray diffraction (XRD). Surface XRD data can be converted into atomic-scale images of epitaxial heterostructures with sub-Ångström resolution along the out-of-plane direction.[9] Fourth generation diffraction limited storage rings allow for unprecedented insights with X-rays into matter as they offer large coherence lengths of 10 to 100 micrometers in the case of hard X-rays allowing for XRD of structures such as grains on this length scale by coherent diffraction imaging.[9] For larger inhomogenous samples, ptychography is used where the beam is scanned with spatial overlap. X-ray laminography[10] is a method that is well suited for flat samples such as integrated circuits and as ptychography allows hierarchical imaging, as we will show in

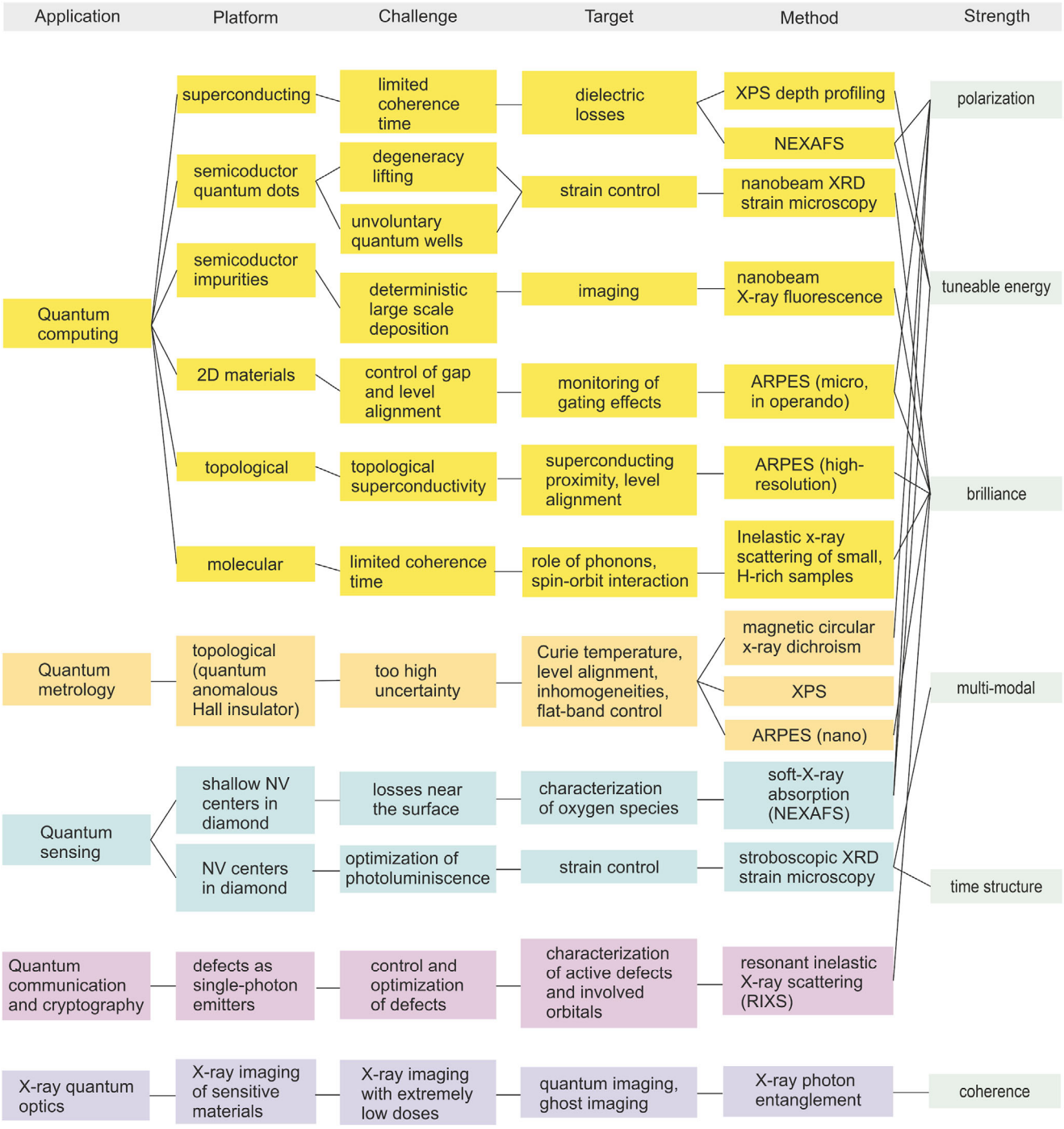

Figure 1. Schematic showing examples for quantum technologies and support by synchrotron radiation methods.

Section 3. We will also demonstrate there how scanning XRD provides strain maps on the nm-scale.

2.3. Spectroscopy

Spectroscopy involves excitation of electrons by X-rays either to a higher energy level or their emission from the sample. The intensity of this transition is measured as a function of incident photon energy (X-ray Absorption Spectroscopy, XAS) or kinetic energy of the emitted photoelectrons (Photo Electron Spectroscopy, PES), or the photon energy of the emitted X-rays (Resonant Inelastic X-ray Scattering, RIXS). The transitions between ground state and final state are specific for element, chemical state, orbital and spin. In the Near-Edge X-ray Absorption Fine Structure (NEXAFS) variant of XAS, the photon energy is tuned through a

core-level energy and probes in this way the element-specific unoccupied density of states. Using electrons (Total or Partial Electron Yield, TEY; PEY) to detect NEXAFS makes the method surface sensitive. We will give an example in Section 4. With variably polarized synchrotron radiation (linear to circular), XAS becomes sensitive to the spin and orbital degrees of freedom. X-ray Magnetic Circular Dichroism (XMCD) as well as X-ray Magnetic Linear Dichroism (XMLD), can deliver element specific spin- and orbital magnetic moments as a function of applied magnetic fields or other external stimuli like laser illumination or radio-frquency excitation. For an example, see Section 3. PES has, as given by the atomic-length-scale escape depth of photoelectrons, a higher surface sensitivity than XAS. The surface sensitivity can be tuned by the kinetic energy via the photon energy and the takeoff angle. Core-level PES even allows for the precise determination of chemical shifts indicating specific bond states of atoms. Angle-Resolved Photoelectron Spectroscopy (ARPES) makes use of momentum conservation and requires crystalline samples. It delivers band dispersions, traditionally at photon energies in the vacuum ultraviolet (VUV) region and is extensively used to study quantum materials. ARPES can also be performed with soft and hard X-rays leading to enhanced bulk sensitivity which allows to probe buried layers. To enhance the contribution of a certain element or chemical shift, ARPES in the soft and hard X-ray range can be performed resonantly at a core level energy. RIXS is also resonant but is a bulk-sensitive technique because emitted photons are recorded. It can also be performed in a momentum resolved way in crystalline solids as complement to neutron scattering. The emitted photons can suffer energy losses due to elementary low-energy charge, spin, orbital and lattice excitations which are probed in this way.[11]

2.4. Spectro-Microscopy

Spectro-microscopy with synchroton radiation down to few nm spatial resolution employs contrast mechanisms from spectroscopy such as XAS in scanning transmission x-ray microscopy (STXM) and ptychography. XMCD and XMLD allow to image spatial magnetic order as a function of external parameters. This holds also for photoelectron emission microscopy (PEEM) recording photoelectrons, Auger electrons or TEY in XAS and XMCD. This is complementary to STXM (film transmission), so that in combination the surface map of films versus bulk can be studied.

2.5. Quantum Science and Technology

Linking synchrotron methods to quantum technology we introduce in the following some of the main scientific and technical questions in the field: A prototypical example of quantum science and technology is quantum computing.[12–16] The research in this field has the objective of ultimately creating a universal and fault-tolerant quantum computer, capable of achieving a significant, ideally exponential, speedup in specific calculations compared to classical computers. An important stimulus has been the theoretical demonstration that Shor's algorithm[17] finds non-trivial divisors much faster than classical algorithms, specifically in polynomial runtime, with profound implications for cryptography. To implement a quantum computer physically requires several preconditions: qubits shall be readable, reliable, and scalable, and they must be initialized and enable a universal set of quantum gates.[18] In recent years, larger-scale yet imperfect quantum computers have become operational, facilitating specific calculations that are challenging for classical machines.

Quantum computing makes use of two basic quantum properties: superposition and entanglement. The wave function of, e.g., an electron spin, can be described by the superposition $\psi = \alpha|0> + \beta|1>$. Hence, differently from classical bits, qubits can exist in states that are "at the same time 0 and 1". As a consequence, a register of N qubits can be prepared in a superposition of any of the 2^N possible combinations of each qubit state, potentially leading to an exponentially larger processing power. Entanglement is a quintessential quantum phenomenon in which the states of two or more systems are correlated so that they cannot be described independently from one another, regardless of their distance. Entanglement is a crucial resource for quantum computing and quantum technologies in general (e.g., it is exploited for quantum error correction and for quantum teleportation) and can occur for instance when two spins interact by an exchange interaction. In quantum computing it is usually created by two-qubit gates (like the controlled NOT or CNOT gate, which controls the entanglement), which typically require a switchable interaction between qubits.

Due to interactions with the environment, quantum states are susceptible to decay and decoherence, which can lead to errors, particularly critical in larger systems with many qubits. Specifically, a superposition of $|0>$ and $|1>$ can decay into a mixture of $|0>$ and $|1>$, effectively destroying the quantum information and halting the computation. The characteristic time of this process is referred to as the coherence time T_2 and has to be as long as possible. Moreover, energy dissipation to the environment within a characteristic relaxation time T_1 is another source of decoherence and limits the coherence time to $T_2 < 2T_1$ for all qubits.[1] Some sources of decoherence, such as inhomogeneous dephasing as measured by T_2^*, can be reduced by special pulse sequences. In general, correcting errors requires many qubits and the implementation of quantum error correction,[19] a crucial milestone to really unleash the full power of quantum computing.

Logic gates are typically implemented by the application of electromagnetic radiation, i.e., microwave or optical pulses. Here, two crucial and connected quantities are the ratio between T_2 and the time needed to implement a gate operation and the fidelity. The has to be very large, ensuring that many gates can be implemented before coherence is significantly affected. The latter, i.e., the accuracy of the physical implementation of the logic transformation, has to be as close to 1 (corresponding to a perfect gate implementation) as possible. The fidelity improves with longer T_2, but also depends on specific characteristics of the used platform. In particular, the fidelity of two-qubit gates depends also on the interaction that generates the entanglement and is generally lower than that of one-qubit gates.[1] Larger-scale systems require consideration of yet other factors. Improving qubit characteristics (like T_2) and the fidelity of quantum gates requires a deep understanding of the hardware and the design of

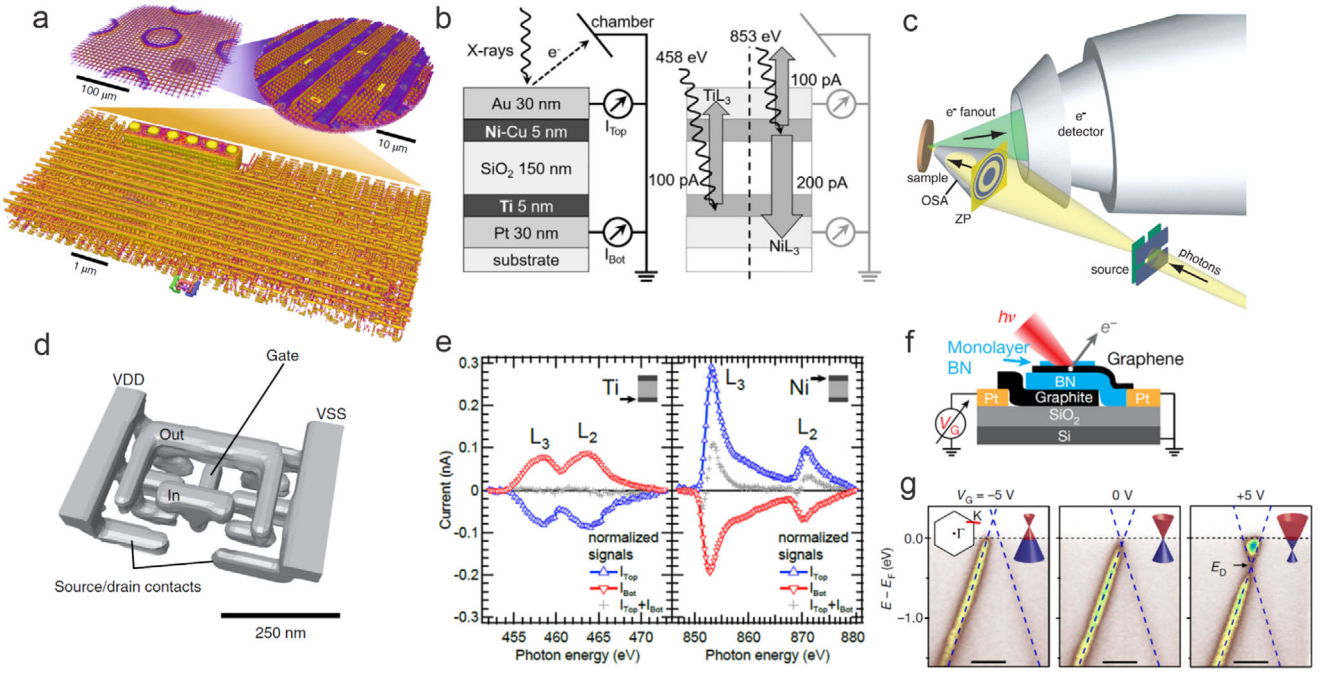

Figure 2. In-operando microscopy and spectroscopy. a, d) Ptychographic X-ray laminography at 6.2 keV of a device allows macro- to nanoscale zoom. Reproduced with permission.[20] Copyright 2019, Springer Nature. b, e) Example of in-operando studies using photoinduced electrical currents. Reproduced with permission.[21] Copyright 2022, AIP publishing. c) Schematic of experiment using angle-resolved photoelectron spectroscopy (ARPES) with submicrometer spatial resolution. Reproduced with permission.[22] Copyright 2010, Wiley. f) Diagram of a 2D heterostructure device for micro-ARPES. g) Micro-ARPES demonstrates the effect of electrostatic gating. A shift of the Fermi level of several 100 meV is observed in the Dirac cone of monolayer graphene by application of a gate voltage. The conduction changes from electron to hole like. Reproduced with permission.[23] Copyright 2019, Springer Nature.

optimized and platform-specific gates. As discussed below and in the subsequent sections, X-rays are a very powerful tool to help in these tasks.

There are various platforms with different strengths, challenges, and perspectives for achieving scalability and error correction. These platforms include superconducting qubits, quantum dots, trapped ions, neutral atoms, molecular qubits/qudits, topological qubits, and photonic quantum computing.

Figure 1 illustrates the links between advanced quantum technologies and various synchrotron radiation techniques discussed above, which we explore through examples in this article. On the right, key properties of synchrotron radiation are listed. In superconducting qubit systems, dielectric losses pose a challenge. X-ray Photoelectron Spectroscopy (XPS) can identify oxide species formed in the dielectric produced by the oxidation of the superconductor, with tunable photon energies enabling depth profiling. A related issue arises in nitrogen-vacancy (NV) centers near diamond surfaces used for sensing, where soft-X-ray absorption is the preferred technique. In semiconductor qubits, spatially resolved strain analysis is critical and can be achieved using nanobeam XRD.

3. Electronic Quantum Devices

A key capability of synchrotron radiation is that it can be used to analyze the structure, properties and function of electronic devices by imaging and in-operando methods, as illustrated in **Figure 2**.

As mentioned above, imaging may be performed in 2D or 3D. Conventional tomography typically prohibits hierarchical imaging since the probed pillar has to be cut out of the sample. This can be avoided by ptychographic X-ray laminography[10] which is well suited for flat samples such as integrated circuits. This has been demonstrated using chips produced with 16 nm fin field-effect transistor technology, achieving a reconstruction resolution of 18.9 nm, see Figure 2a,d.[20]

In the center part of Figure 2, a new method of soft-X-ray absorption spectroscopy is employed.[21] Instead of the conventional TEY, a two-channel TEY is introduced in which the photocurrents from two electrodes are recorded via tracer layers of the two elements Ni (top electrode) and Ti (bottom electrode), which can be distinguished in the spectra. At the Ti L-edge, electrons are excited in the Ti layer and may diffuse across the SiO_2 dielectric layer. The currents in the bottom and top electrode compensate each other. At the Ni L-edge, the electrons are excited at the top electrode leading to a current with opposite sign. Moreover, some of the photoexcited electrons from the Ni can reach the surface and contribute to external photoemission which leads to an imbalance in the currents from the top and bottom electrodes. This shows that internal photoexcited currents in selected buried layers and interfaces at distances up to at least 185 nm from the surface can be probed.[21]

ARPES probes electronic band dispersions $E(k)$ of occupied states and, as mentioned above, is a method of high surface sensitivity (a few atomic layers). It has recently been extended to in-operando methods enabling the application of electric, magnetic,

and strain fields, electric currents and gate voltages.[24] This extension involves first of all a high spatial resolution in the micrometer or submicrometer range. Figure 2g shows the strong effect of electrostatic gating on monolayer graphene[23] (see also ref. [25]), which is particularly susceptible due to its small density of states around the Dirac point, the crossing point of the linear $E(k)$ dispersion. The Fermi level shifts across the Dirac point while the dispersion of the Dirac cone itself does not change.

After these examples of electronic devices employing conventional (Ni and Ti) and quantum materials (graphene), we will in the following show how various synchrotron- and FEL-radiation methods are used to characterize the electronic, chemical, and magnetic properties of these materials and their functionality with applications in quantum computing and quantum metrology.

3.1. Quantum Computing

3.1.1. Superconducting Qubits

Superconducting quantum computers have been at the center of most recent breakthroughs such as the 53 qubit quantum computer outperforming the largest classical computers in calculating a random circuit.[26] Superconducting qubits rely on superconducting circuits to encode and manipulate quantum information. In 2004, a superconducting artificial atom was coherently coupled to a microwave frequency photon in the strong-coupling regime.[27] This established circuit quantum electrodynamics as an analog of cavity quantum electrodynamics which employs atoms and quantum optics. For a review see ref. [28]. Superconducting circuits are fabricated on silicon or sapphire substrates using silicon CMOS techniques and materials. The process involves lithographic patterning, metal deposition, etching, and controlled oxidation of thin films of a superconductor such as aluminum or niobium. They are electrically shielded and cooled to 10 mK.[28,29] The quantum harmonic oscillator consists of a resonant circuit with a capacitor and an inductor, resonating at frequency $\omega_c = 1/\sqrt{LC}$. The quantized energy levels are spaced by ω_c. Typically the lowest two levels are used as qubit ($|0>$ for the ground state and $|1>$ for the excited state). In order to address each transition uniquely and avoid excitations to higher levels, an anharmonic potential is created by a Josephson junction.[29] The parameters of the circuit can be tuned and the ratios of the Josephson energy, the capacitive charging energy, and the inductive energy allow to engineer qubit properties such as transition frequency, anharmonicity, and sensitivity to various noise sources.[29] Two important qubit types are the charge qubit and the magnetic flux qubit.

The sources of loss and noise in the materials are insufficiently understood. The transmon qubit (transmission line shunted plasma oscillation qubit),[31] which is of the charge qubit type, has reduced sensitivity to charge noise because a shunting capacitor lowers the charging energy relative to the Josephson energy so that the energy level spacings are almost independent of offset charge. It is believed that the lifetimes of existing 2D transmons are limited by microwave dielectric losses.[32,33] Ta-based planar transmon qubits can exhibit record lifetimes $T_1 > 0.3$ ms (and > 0.23 ms in average),[32] three times larger than achieved with Nb and Al-based ones.[33,34] It was estimated that the advantage of Ta is its robust, stoichiometric oxide, which is resistant to a wide range of aggressive chemical processes while the amorphous non-stoichiometric oxide layer at the surface of Nb and Al is a plausible source of dielectric loss arising from two-level systems, characterized by charges or atoms tunneling between two metastable states.[1]

For depth profiling of bcc Ta(111) films with a thin oxide layer, the excitation energy of Ta 4*f* core.level spectra has been varied in XPS between 630 and 6000 eV, see **Figure 3**c,d,e.[30] This is a requirement that can only be met with a synchrotron-radiation beamline that covers the soft-to-tender energy range. It was shown that the Ta surface is dominated by Ta_2O_5, which is the fully oxidized case, but at the interface to the Ta, suboxides with Ta^{3+} and Ta^{1+} were detected. The Ta oxide layer was thinner with sharper interfaces than what was found for Nb oxide, which was studied with photon-energy dependent core-level spectroscopy as well.[35] This difference could explain the improved performance of Ta-based superconducting qubits.[30] Comparison to systematic studies of the microwave dielectric loss for different surface conditions of the Ta devices[36] indicated Ta^{3+} as the origin of the dielectric loss currently limiting the devices.[30] With the XPS analysis applied to different acid treatments, it was possible to grow the Ta oxide in a controlled way and thinner than previously achieved.[30]

3.1.2. Semiconductor Qubits

Prominent semiconductor qubits which use the spin are the quantum-dot qubit and the donor qubit. For a review see ref. [37]. In a semiconductor, a quantum dot can be defined by voltages on gate electrodes. The qubit is then stored in spin states of the quantum-confined electrons or holes. Using the spin states of coupled single-electron quantum dots, Loss and DiVincenzo proposed a universal set of one- and two-qubit gates for quantum computation.[38] In the two-qubit quantum gate, the single spin qubit can be controlled by resonant microwave pulses while two qubits couple through the exchange interaction, which can be tuned by electrically gating the tunneling barrier. The exchange interaction is a combined effect of the Pauli exclusion principle and the Coulomb interaction. Between quantum dots, which are too far away for a direct orbital overlap, the exchange is controlled via tunneling.[37] The tunability of the exchange coupling with a gate voltage has been demonstrated[39] and enables time-dependent control for implementing entanglement in two GaAs quantum-dot qubits.[40] A single-electron transistor is used for readout. The length scale of the confinement and electrodes is 10–100 nm which is orders of magnitude smaller than for superconducting qubits and is reached by electron lithography.[41] Enrichment of the spin-zero ^{28}Si isotope reduces the spin decoherence by hyperfine interaction with nuclear magnetic moments when ^{29}Si atoms are absent in the active region of the device. Two-qubit CNOT gates have been realized in ^{28}Si enriched Si.[42]

Although silicon quantum-dot qubits largely avoid nuclear spin noise in this way, electric field noise is a problem for single- and multi-qubit operations.[43] It was found that charge noise increases with the thickness of the aluminum-oxide gate dielectric,[43] suggesting the necessity for a

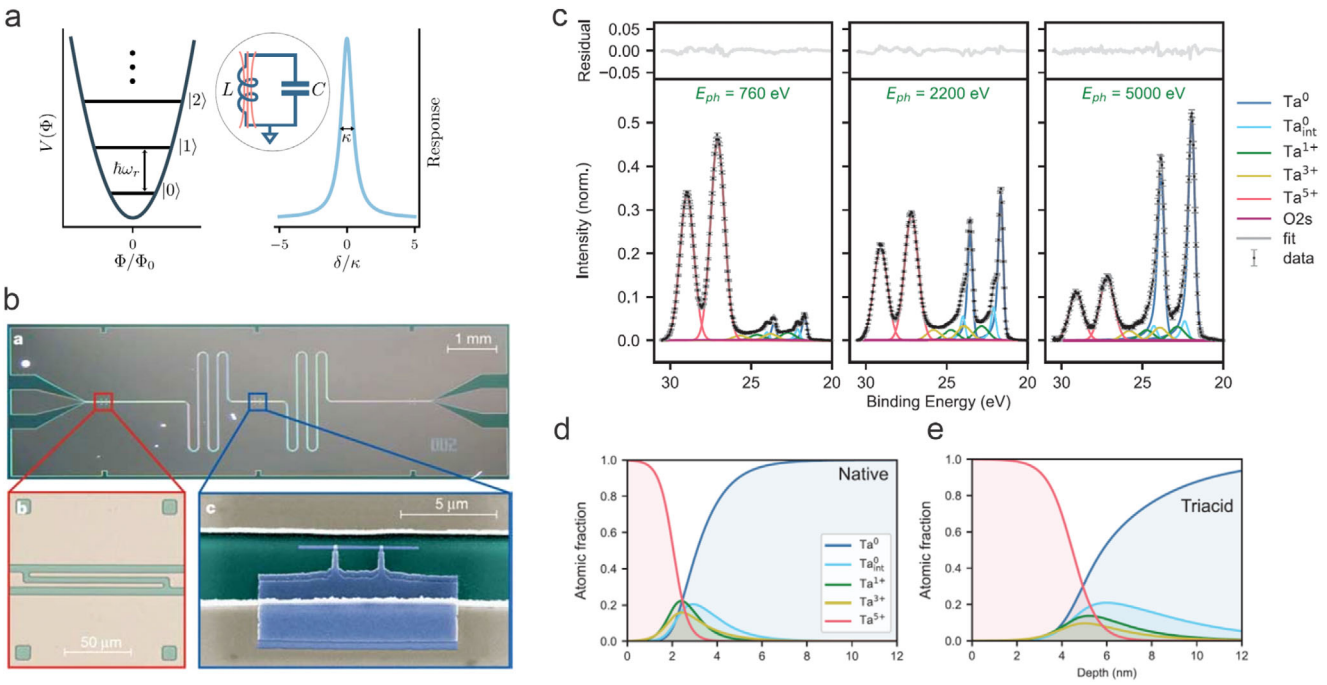

Figure 3. Superconducting qubits. a) Harmonic potential versus flux of the *LC* circuit (inset). Response of the oscillator to an external perturbation as a function of detuning δ. $\kappa = \omega_r/Q$ is FWHM with the quality factor Q. $1/\kappa$ is the average lifetime of the single-photon state $|1>$ before it decays to $|0>$. Reproduced with permission.[28] Copyright 2021, American Physical Society. b) Integrated circuit for cavity quantum electrodynamics. (b-a) Superconducting Nb resonator. (b–b) Input–output feedline at each end of the resonator. (b-c) Cooper pair box from Al. The Josephson tunnel junctions are formed at the overlap between the long thin island parallel to the center conductor and the fingers extending from the reservoir. Reproduced with permission.[27] Copyright 2004, Springer Nature. c, d, e) Depth profiling of the oxide dielectric of superconductor qubits for loss control. The sharp *4f* core level of Ta allows precise assignment of oxidation states. The wide photon-energy range offered by synchrotron radiation allows for depth profiling by variation of the probing depth over a wide range. Different acid treatments are compared that expose only the stable stoichiometric oxide. Adapted under the terms of CC BY 4.0 license.[30] Copyright 2023, Wiley-VCH.

similar control as mentioned in Section 3.1.1 for superconducting qubits. Temperature-dependent noise magnitude and spectrum vary among quantum dots implying that charge noise in Si/SiGe quantum dots likely stems partially from a nonuniform distribution of two-level systems near the surface of the semiconductor.[43]

Shortly after the Loss-DiVincenzo proposal, Kane introduced a concept using the nuclear spins of ^{31}P donor atoms in Si as qubit.[44] ^{31}P electron- and nuclear-spin qubits in a top-gated nanostructure on a ^{28}Si substrate have led to ^{31}P nuclearspin coherence time > 30 s (single qubit) and > 99.99% control fidelity and electron-spin coherence time > 0.5 s.[45] Group V donors in Si such as P are hydrogen-like and feature a loosely-bound single spin-1/2 electron. This situation is similar to free alkali atoms (used in atomic clocks), however, the high dielectric constant and low effective mass of the Si host lead to a much smaller binding energy of several 10 meV and a much larger Bohr radius, which is the general basis of doped semiconductors and p-n junctions.

To form quantum gates, the states have to evolve coherently. Instead of control of interaction by gate electrodes, in the Stoneham-Fisher scheme[48] the coupling is achieved via optically induced electronic excitation. To avoid the coupling in the ground state, appropriate spacings, e.g. 10 nm for the deep donor Bi in Si, are sufficient.[48]

Using THz coherent synchrotron radiation from an FEL, it has been demonstrated that tunneling between P and Sb atoms can be controlled by selective photoexcitation of either P or Sb atoms at 10 K.[49] The large Bohr radius reduces the spin-orbit coupling. THz radiation from the FEL has also been used to reveal that the spin-orbit coupling is small enough to preserve the spin during an excitation and phonon relaxation cycle.[50] This is important for qubit and quantum-sensor applications where THz excitations initiate either a coupling or a readout sequence.[50] The coherent manipulation of the electron-spin qubit in a P atom in Si is achieved by microwaves. This, as well as its electrical readout, has been demonstrated with a large $T_2 > 200$ μs.[51] An orbital qubit, corresponding to the 1s →2p transition, requires THz radiation. **Figure 4a**, b shows how the transition is achieved with pulsed FEL radiation.[46] The sequence of two Ramsey pulses, the representation in the Bloch sphere, and the *y*-component of the Bloch vector displaying Ramsey fringes are shown. A coherence time $T_2^* = 160$ ps is measured for 10^5 atoms at liquid He temperature.

Single-donor qubits in Si are routinely formed using ion implantation and have been characterized as the basis for a viable platform for quantum computing. As the next step, the creation of patterned arrays of donor qubits for controlled coupling is considered.[52] Again, two qubits couple by the exchange interaction, which needs to be switched on and off over orders of magnitude.[53] The modeling of the exchange interaction between two donor electrons is rather complex due to multi-valley interference effects which requires a precise knowledge of the

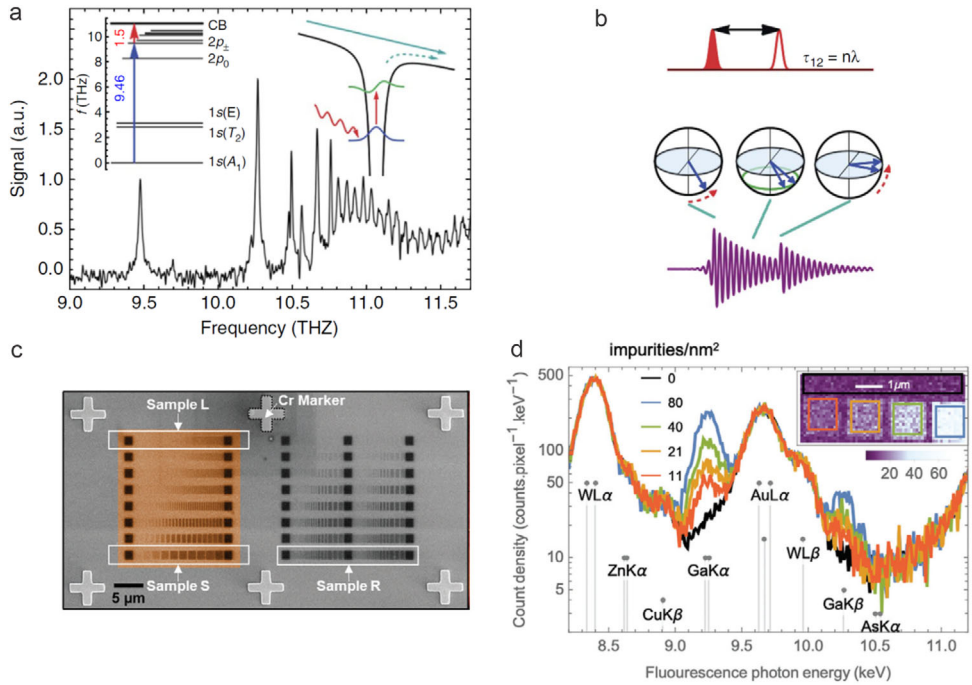

Figure 4. Impurities in Si for qubits. a,b) Coherent manipulation of the 1s →2p two-level quantum oscillator of P by pulsed FEL THz radiation and electrical readout by photothermal ionization. Amplitude and relative phase of the coefficients of the superposition are represented in the Bloch sphere. The *y*-component of the Bloch vector, representing the polarization, displays Ramsey fringes. $T_2^* = 160$ ps was determined for 105 P atoms in Si. Reproduced under the terms of CC BY 4.0 license.[46] Copyright 2015, Springer Nature. Bottom: X-ray fluorescence (XRF) can detect implanted Ga impurities in Si with a sensitivity of currently 650 Ga impurities. c) Scanning electron microscopy image of the implanted regions. d) XRF of sample "S" (marked on the left). Reproduced under the terms of CC BY 4.0 license.[47] Copyright 2024, Wiley-VCH.

distance. Anti-correlated spin states have been measured for two phosphorus spin qubits in Si separated by 16±1 nm.[53] This arrangement has been achieved with scanning tunneling microscopy lithography which uses a hydrogen monolayer as resist.[14] Single ion implantation is the closest competitor of this method with precision in the order of 10 nm and faster as well as more flexible in terms of impurity species and host.[54] For these larger length scales that also facilitate addressing and manufacturing, new gating schemes with much larger allowable spacing between the qubits have been devised.[55,56] These will require appropriate diagnostics and imaging of the structures produced, including by X-ray methods. Recently, Ga implantation in Si for spin-3/2 qubits, which is also used for creating p-type contacts, has been studied by synchrotron-radiation-based X-ray fluorescence (XRF).[47] The sensitivity was enhanced by the use of nanobeams to detect 650 Ga impurities, which means an about 30 times higher sensitivity than achieved previously, see Figure 4c,d. It is expected that after further instrument upgrades, single atom detection by synchrotron-radiation-based XRF is within reach.[47] The detection of single impurities using fluorescence could be useful in probing variations in the bonding configuration around individual atoms using NEXAFS.[47]

Synchrotron-radiation-based ARPES has been applied to buried P atoms 2 nm beneath the surface of Si.[57] It was possible to probe the band dispersion of the created 2D electron gas even beyond the small probing depth of the photoemission experiment in the VUV photon energy range.[57] δ -doping of Si with As and P atoms up to 4 nm beneath the surface has also been investigated with soft-X-ray ARPES at an enhanced probing depth.[58] The ARPES intensity oscillation as a function of photon energy has allowed determination of the electronic wavefunction localization over the doped δ -layer, yielding an electronic thickness of 0.45±0.04 nm.[58]

Strain effects are crucial in quantum-dot qubits. Because Si has multiple conduction-band valleys, tensile strain is being employed during growth.[2] Large in-plane strain lifts the energies of in-plane *x,y* valleys, and the remaining twofold degeneracy of the *z* valley is lifted by the quantum well itself to a splitting of 0.1 to 1 meV, which is very delicate. For dopants in Si, the valley degeneracy is lifted by the strong confinement potential from the dopant, for P resulting in 11.7 meV splitting.[59] Moreover, strain from gate electrodes affects the performance and, when carefully characterized, provides a new axis for device design. While the gates define the electrostatic potential of the dots, the imposed stress is transferred so deep that it affects the active region of the device. Typical strains from metal gates are large enough to create strain-induced quantum dots rendering strain as important as electrostatics for the operation of the quantum-dot device. Nanobeam XRD has been used to study strain effects of metallic gate electrodes on quantum dots in Si[60] and GaAs structures.[61] Combined with dynamical modeling the measurements reveal lattice tilts up to 0.04° and strain around 10^{-4} in the 2D electron gas (2DEG) of GaAs/AlGaAs heterostructures.[61] Elastic distortions modify the 2DEG's potential energy landscape via deformation potential and piezoelectric effects. Investigations of individual linear electrodes reveal lattice tilts consistent with a 28

MPa compressive residual stress in the electrodes.[62] The angular magnitude of the tilts varies by up to 20% over distances of less than 200 nm. In multiple-quantum-dot devices, where also the electrodes are more complex, such variations occur as well and can lead to significant challenges but possibly also opportunities for scaling.[62] Recently, strain tensor components were also laterally resolved for Si/SiGe[60] and Ge/SiGe[63] quantum wells in a device at a lateral resolution of 50 to 60 nm.

Graphene is a potential alternative to Si for quantum-dot qubits. Spin decoherence is reduced due to the low spin-orbit interaction of carbon and due to the fact that only 1% of carbon isotopes (^{13}C) carry a nuclear magnetic moment. Additionally, the valley degeneracy of bilayer graphene provides an extra degree of freedom for qubit realization.[64] Valley state relaxation times are over an order of magnitude longer than spin relaxation times.[65] Graphene quantum dots have been demonstrated using bilayer graphene encapsulated in hexagonal boron nitride (hBN) layers.[64] A perpendicular electric field opens a bandgap in bilayer graphene, demonstrated at first by ARPES with synchrotron radiation.[66] The control of the gap by gating enables the formation of tunable multi-quantum-dot systems. In this way, triple quantum dots have been demonstrated in bilayer graphene.[67] With micro- and nano-ARPES, electronic band structures can be probed at sub micron spatial resolution.[24] Moreover, this spatial resolution allows to monitor local changes in the electrical potential and the Fermi level while a gate voltage is applied which makes micro-ARPES an in-operando method as shown already in Figure 2g.

While the low spin-orbit interaction in graphene due to the low atomic number of carbon is an advantage leading to low spin decoherence, other 2D materials with higher spin-orbit interaction would enable faster operation of spin qubits. Transition-metal dichalcogenides have larger bandgaps (1.5 to 2.5 eV) than bilayer graphene. Like with graphene, quantum dots can be defined by electrostatic gating. A quantum dot of seven-layer WSe_2 has been demonstrated.[68] In-operando ARPES can reveal band bending and the change of the band structure upon gating. For monolayer WSe_2, the gap increases by several 100 meV upon application of the gate voltage.[23]

3.1.3. Topological Qubits

Topological qubits shall enable fault-tolerant quantum computation. The quantum gates involve the braiding of degenerate non-Abelian anyons. The fault tolerance stems from the fact that the unitary transformations resulting from braiding depend only on the topological class of the braid rendering the encoding and processing of quantum information nonlocal.[69] The topological immunity is protected by an energy gap and a length scale.[70] One realization of the non-Abelian anyon is a Majorana zero mode, i.e., a midgap excitation.

Different material platforms for Majorana zero modes have been suggested such as GaAs/AlGaAs quantum wells for a $\nu = 5/2$ fractional quantum Hall system[71] and the proposed $p_x + ip_y$ superconductor Sr_2RuO_4[72] which has extensively been studied by ARPES[73] but has not been confirmed as p-wave superconductor. ARPES plays an important role in investigating other material candidates. Another platform is a quantum anomalous Hall (QAH) insulator in contact with an s-wave superconductor. For this arrangement a chiral Majorana zero mode is predicted[74] and a braiding procedure for 1D Majorana zero modes has been proposed.[75] Early reports of the observation of chiral Majorana zero modes via half-integer Hall plateaus could not be confirmed. Reproduction of 30 samples did confirm the half-integer Hall plateaus but unlikely caused by chiral Majorana zero modes.[76] We will further discuss the QAH insulator in the context of quantum metrology in Section 3.2.

A topological superconductor may as well be induced at the interface of conventional materials. The currently favored platform is a semiconductor nanowire structure in contact with a superconductor.[77,78] The superconductor is conventional (s-wave) and the semiconductor must have a strong Rashba-type spin-orbit interaction which is gapped at the Kramers point by an external magnetic field. Evidence of Majorana zero modes in InSb nanowires has been claimed in 2012.[79] The zero bias peak is at least consistent with an interpretation as Majorana zero mode. However, outstanding next steps are the proof of exponential localization at the ends of the wire and the non-Abelian braiding. One of the challenges is the growth and characterization of the nanowire.

Cylindrical nanowires can be grown by electrochemical deposition inside channels of ion-track-etched polymer membranes. Bi_2Te_3 nanowires with 100 nm diameter have been investigated individually with nano-ARPES.[80] At 100 eV photon energy a spatial resolution of 120 nm was achieved in ARPES as well as in core-level spectroscopy.

Heterostructured semiconductor nanowires are important for various quantum effects. Core-multishell GaAs/AlAs nanowires have been grown which incorporate a quantum ring structure. They are a suitable platform for manifestations of the Aharonov-Bohm effect of neutral and charged excitons.[81] For Majorana devices,[79] in addition to the material requirements for bandgap and mobility met by InSb, the nanowire geometry and electronic quality pose challenges, such as diameter below 100 nm and length of several micrometers and a few 100 nm electron mean free path.[82]

Simulations predict more complex strain distributions and higher strain tolerance in nanowires than in 2D films.[83] This is due to strain relaxation at the surface but has been difficult to investigate experimentally so far. Both radially and axially heterostructured nanowires can be studied by scanning XRD. Recently, an axially segmented GaInP-InP heterostructured nanowire with 190 nm diameter has been investigated, see **Figure 5** (a,b).[83,84] From segments with length from 45 to 170 nm, strain maps with 0.01% relative strain sensitivity have been obtained which would be challenging to quantify with transmission electron microscopy.[83] Strain maps are derived from the local deviation of the lattice constant. The total range of measured strain is about 0.14% (InP segments) and 0.42% (GaInP segments).[83] The InP segments are compressively stressed by the GaInP segments in the radial direction so that they should intuitively be expanded in the probed axial direction. However, the strain distribution turns out significantly more complex. While the shortest InP segment practically adapts to the surrounding GaInP segments, the two larger segments reveal indeed the lattice expansion in the axial direction near the surface but away from the surface the strain is compressive.[83] In addition to

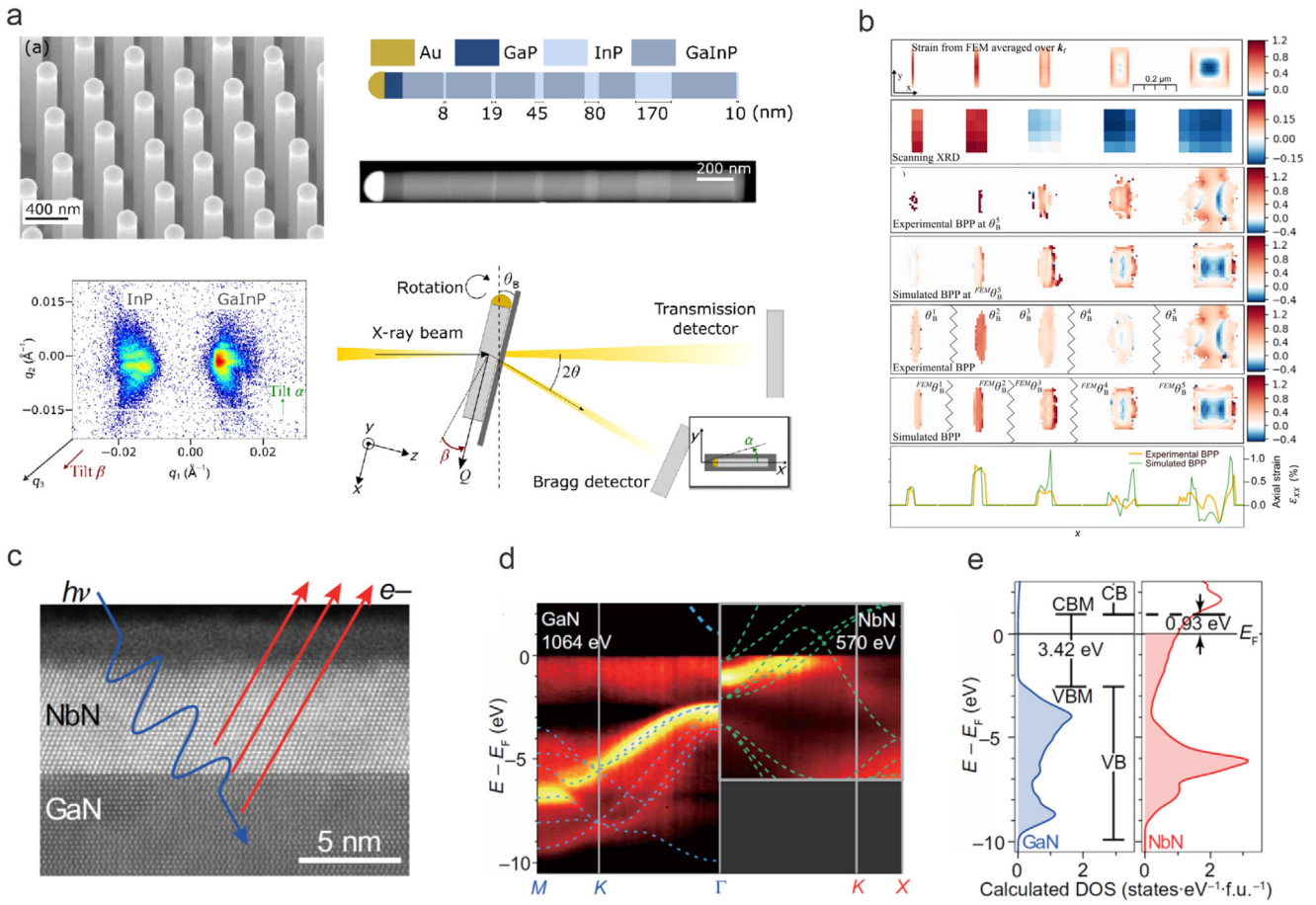

Figure 5. Semiconductor nanowires and interfaces. a,b) Scanning X-ray diffraction and Bragg projection ptychography. Experimental results and simulations of a single heterostructured nanowire. (a) Reproduced under the terms of CC BY 4.0 license.[83] Copyright 2020, Springer Nature, (b) Reproduced under the terms of CC BY 4.0 license.[84] Copyright 2024, Wiley-Blackwell. c, d, e) Soft-x-ray ARPES to determine the momentum-resolved band offset at a buried superconductor-semiconductor interface. Reproduced under the terms of CC BY 4.0 license.[85] Copyright 2021, American Association for the Advancement of Science.

the strain, small variations in the local lattice tilt are resolved (Figure 5a). Most recently, 2D Bragg ptychography has been used to produce higher resolution images of the nanowire (40 nm resolution compared to 100 nm with nano XRD). This also offers improved strain resolution, see Figure 5b.

The enhanced probing depth of ARPES in the soft-X-ray range allows it to probe buried layers. Epitaxial films of superconducting NbN on semiconducting GaN have been probed by this method,[85] see Figure 5c,d,e. The Schottky-barrier height obtained from photoemission was found to be in agreement with electronic transport and optical measurements.[85] Most importantly, the Fermi level states in NbN involved in the superconductivity, turned out to be offset in momentum space from the states at the valence-band maximum in the GaN and therefore do not hybridize with them. Excluding potential poisoning of the superconductivity, this experimental finding puts forward the prospect of NbN/GaN heterojunctions for quantum devices.[85]

Superconductivity is modified on the nanoscale, e. g., the critical temperature of Sn increases by up to 10% in nanostructures. In order to distinguish electronic from phononic effects, modifications of the phononic structure can be probed by synchrotron radiation. Nuclear inelastic scattering probes the phonon density of states by excitation of nuclear levels with highly monochromatic X-rays (e.g., 23.8 keV with sub-meV resolution for ^{119}Sn) and measurement of the deexcitation.[86,87] Intriguing is also the enhancement of the critical temperature of FeSe at interfaces, e.g. with $SrTiO_3$.[88] The electron-phonon coupling in FeSe could be studied in detail by coupling ultrafast photoemission and XRD. XRD with an X-ray FEL tracks the light-induced femtosecond coherent lattice motion at a single phonon frequency, and photoemission monitors the subsequent coherent changes in the electronic band structure.[89]

We mentioned above the QAH insulator in contact with an *s*-wave superconductor. The proximity of a topological insulator and the *s*-wave superconductor is expected to lead to a topological superconductor. To study the superconducting proximity effect, Bi_2Se_3 topological insulator films have been grown on superconducting $NbSe_2$,[90] **Figure 6a**. Six quintuple layers of Bi_2Se_3 were needed to avoid hybridization of top and bottom layers, which is required to maintain the nontrivial topology. The superconducting gap was confirmed by scanning tunneling spectroscopy.[90] ARPES is needed to determine the position of the chemical

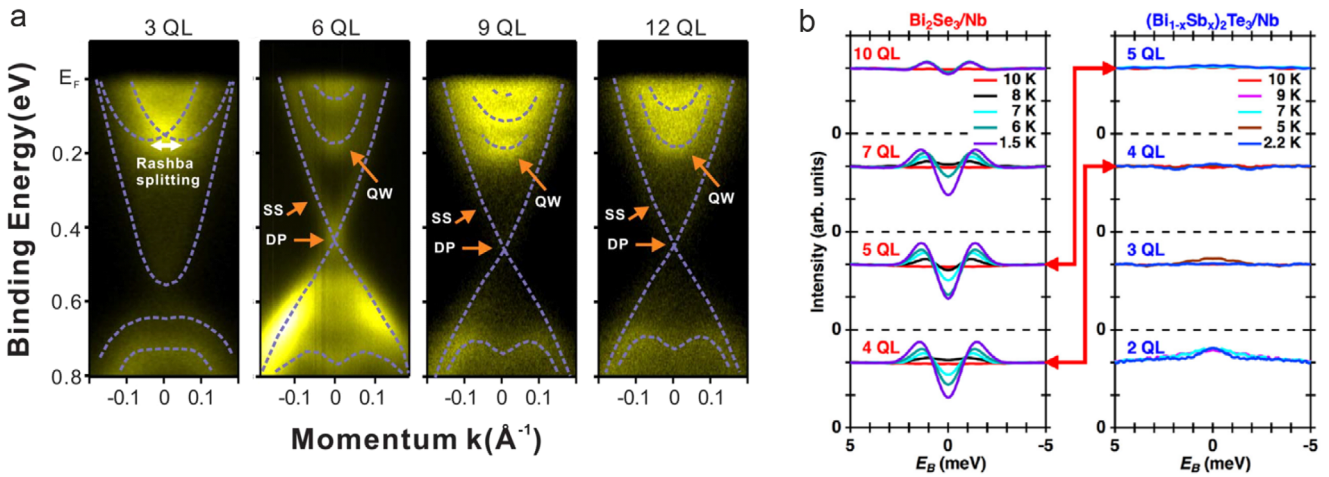

Figure 6. Superconducting proximity for topological qubits. a) Proximity between an s-wave superconductor and a topological insulator can be used as a building block for a topological qubit. ARPES can judge the presence of the nontrivial topology, of the superconducting gap, and of the energetic alignment of the gaps. Six quintuple layers of Bi_2Se_3 on $NbSe_2$ are confirmed to remain topological. Reproduced with permission.[90] Copyright 2012, American Association for the Advancement of Science. b) Symmetrized ARPES spectra of interfaces of n-doped Bi_2Se_3 and bulk insulating $(Bi_{1-x}Sb_x)_2Te_3$ with superconducting Nb indicate that bulk states are required to transmit the superconductivity to the surface of the topological insulator. Reproduced with permission.[91] Copyright 2020, American Physical Society.

potential because the superconducting gap and the gap of the topological insulator need to be aligned. Recently, Bi_2Se_3 has been compared to bulk insulating $(Bi,Sb)_2Te_3$ on Nb metal,[91] see Figure 6b. It was concluded that bulk states are required to transmit superconductivity to the surface of the topological insulator.

3.1.4. Molecular Qubits

Molecular spins can be employed for quantum computation, quantum simulations and sensing.[15,92–95] In contrast to the approaches discussed above, chemical synthesis can enable bottom-up creation of quantum systems taking full advantage of the quantum properties on the atomic length scale.[94] Many interesting and complex structures were realized, achieving a remarkable degree of control on the Hamiltonian and coherence times. In particular, coherence times close to a millisecond were observed at low temperatures in a vanadium complex and supramolecular structures containing a significant number of qubits were investigated.[15] Often the magnetic core of molecular spins contains few magnetic ions coupled by exchange and dipolar interactions. Transition-metal, lanthanide, and actinide ions as well as organic radicals were exploited as building blocks of magnetic molecules. For instance, the entanglement between two molecular qubits, each containing eight interacting transition metal ions, was investigated by neutron scattering.[96]

An emerging characteristic of molecular spins that is very interesting for quantum technologies is the fact that they are typically characterized by a sizable number of low-energy states that can be coherently manipulated. Hence, these molecular systems enable one to use d different levels and define qudits (quantum states in d-dimensional Hilbert space), thus adding flexibility for quantum technologies. For instance, it has recently been shown that it is possible to encode a logical qubit protected by quantum error correction into a single molecular qudit,[15] thus possibly circumventing the explosion in the number of physical qubits typical of most quantum error correction codes. Another interesting application of molecular qudits is related to quantum simulations, where the use of qudits can reduce the number of error-prone two-qubit gates. The first working quantum simulator based on molecular qudits has recently been demonstrated.[97]

Synchrotron-radiation-based techniques can help in addressing key issues for molecular qubits and qudits, ranging from the characterization of molecules to the understanding of quantum phenomena and relaxation. A controlled deposition of a monolayer of molecular qubits on a surface is often a mandatory step for quantum devices. However, key issues can arise from the possible unwanted changes in the spin Hamiltonian during this deposition. Here, XMCD is an invaluable tool to characterize the Hamiltonian of molecules in the monolayer. For instance, the magnetic anisotropy of individual molecules in the monolayer was investigated as a function of the orientation of the applied magnetic field.[98] The findings were found in good agreement with spin Hamiltonian simulations, confirming that the deposited molecules preserve the main characteristics of their Hamiltonian. Another interesting use of synchrotron-radiation-based spectroscopic techniques in molecular spins was the detection of resonant quantum tunnelling of the magnetization in a monolayer.[99]

A noteworthy recent result was obtained on the $Fe(pypypyr)_2$ (pypypyr = bipyridyl pyrrolide) molecule. This is a newly synthesized low-spin ($S = 0$) complex that can be evaporated in vacuum. NEXAFS at the Fe L_3-edge (709 eV) is very sensitive to the spin state of Fe(II) compounds. At 8 K, the soft-x-ray illumination together with 2.38 eV visible light creates a second intense feature, characteristic of the high-spin state, see **Figure 7**a.[100] While the low-spin state is without illumination stable up to at least 510 K, the light-induced high-spin state ($S = 2$) has a lifetime of several hours (Figure 7b[100]), orders of magnitude more than would have been expected based on the inverse energy

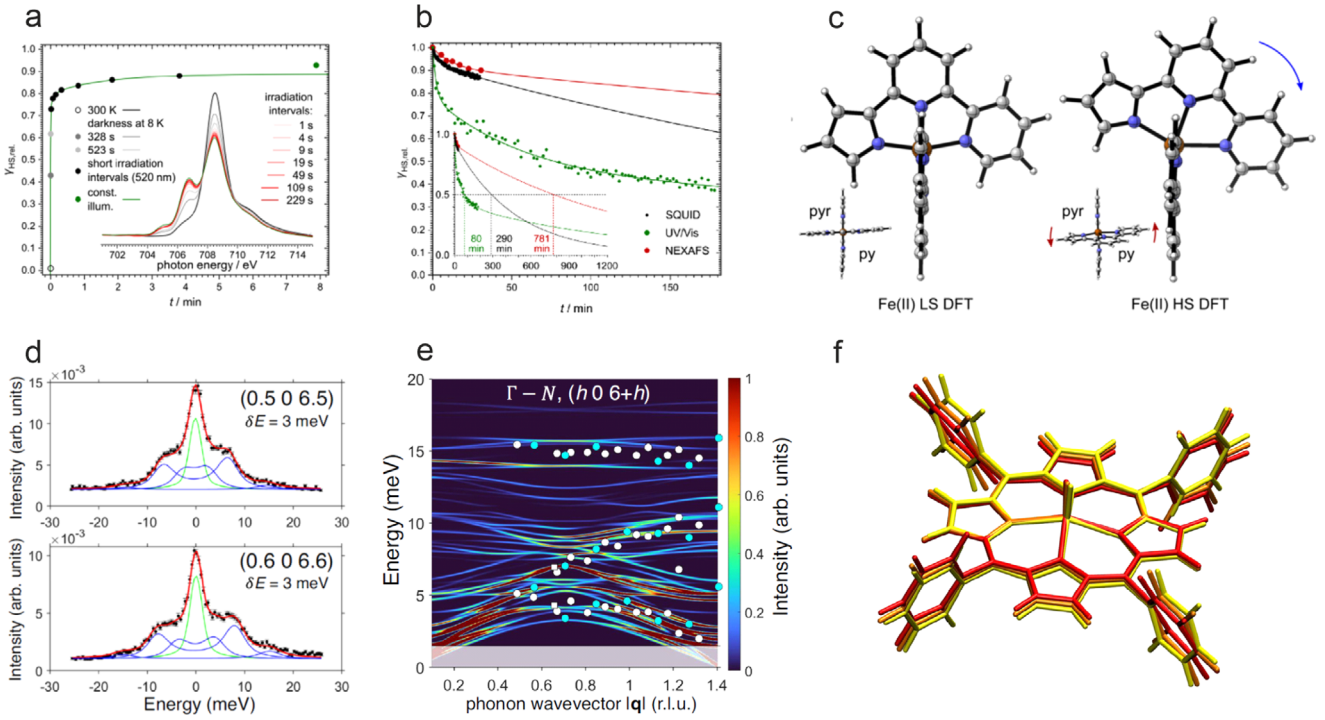

Figure 7. Molecular magnets. a,b,c) Near-edge X-ray absorption fine structure allows distinguishing high- and low-spin states of an Fe(II) complex and reveals a very long lifetime of the light-induced high-spin state. Reproduced under the terms of CC BY 4.0 license.[100] Copyright 2023, RSC Publishing d,e,f) Inelastic X-ray scattering for phonon dispersions of a vanadyl porphyrin complex molecular qubit molecule. Vibrations with very low phonon energy are identified as a reason for spin relaxation. Large (red) and small distortion (orange) associated with the first optical mode at the Γ-point are shown versus the equilibrium structure of the molecule (yellow).Reproduced under the terms of CC BY 4.0 license.[102] Copyright 2023, Springer Nature.

gap law.[101] This is explained by a structural rearrangement, see Figure 7c.[100]

A critical point of most quantum technologies is to reduce relaxation and increase the coherence times of qubits. The main source of relaxation in molecular spin qubits and qudits are vibrations. In order to reduce spin relaxation and decoherence due to vibrations, it is important to understand the relevant vibrations and their coupling to spins.[102] To this end, a radiation-robust vanadyl porphyrin complex has been studied. This spin system is a promising molecular qubit/qudit, and it forms also dimeric species where the two electronic spins are distinguishable and exchange coupled to implement quantum gates.[103] Inelastic x-ray scattering (IXS) for phonon dispersions along the main symmetry directions of the crystal was conducted as well as spin dynamics simulations by density functional theory, see Figure 7d,e,f.[102] IXS was used for the first time on a molecular nanomagnet. The advantage over neutron scattering is that a small crystal can be used and that molecules with high H concentration can be probed. Intra-molecular vibrations with very low energies of 1–2 meV are identified as responsible for spin relaxation, see Figure 7d,e,f.

3.2. Quantum Metrology

The quantum Hall effect provides quantization of the Hall conductance with integer multiples of e^2/h[104] and hence plays an important role in metrology.[105] The QAH effect allows the observation of nonzero integer Hall conductance without external magnetic fields provided typically by superconducting magnets. The QAH effect has been realized for the first time with the advent of topological insulator materials.[106] ARPES is used to verify the nontrivial topology, which is particularly relevant when the chemical composition is modified by magnetic doping, see **Figure 8**, and also the status of charge doping which is critical for the transport signature.[107] The QAH effect has been demonstrated in epitaxial films of the ferromagnetic topological insulator Cr-doped $(Bi,Sb)_2Te_3$.[106] With respect to its metrological applications, in films of V-doped $(Bi,Sb)_2Te_3$, a quantization of the Hall resistance that deviates from the von Klitzing constant h/e^2 by only 0.17 ± 0.25 ppm has been achieved at zero magnetic field.[108] For a quantum resistance standard, however, an uncertainty on the order of 1 ppb is required[109,110] which demands further progress in materials science of QAH insulators.

Materials limitations concern the low operation temperature of 1 K in Cr- and V-doped $(Bi,Sb)_2Te_3$, connected to the disorder due to random magnetic doping. XMCD and resonant photoemission[111] at the vanadium L-edge have been used to characterize the magnetic and electronic properties of these systems element specifically.[112,113] Details of the bulk bandgap formation that may explain the limited operation temperature have been revealed by ARPES, see Figure 8g.[114] With the discovery of intrinsic, i.e., stoichiometric, ferromagnetic topological insulators[115] it has been possible to overcome this temperature limitation, see Figure 8c,d. In

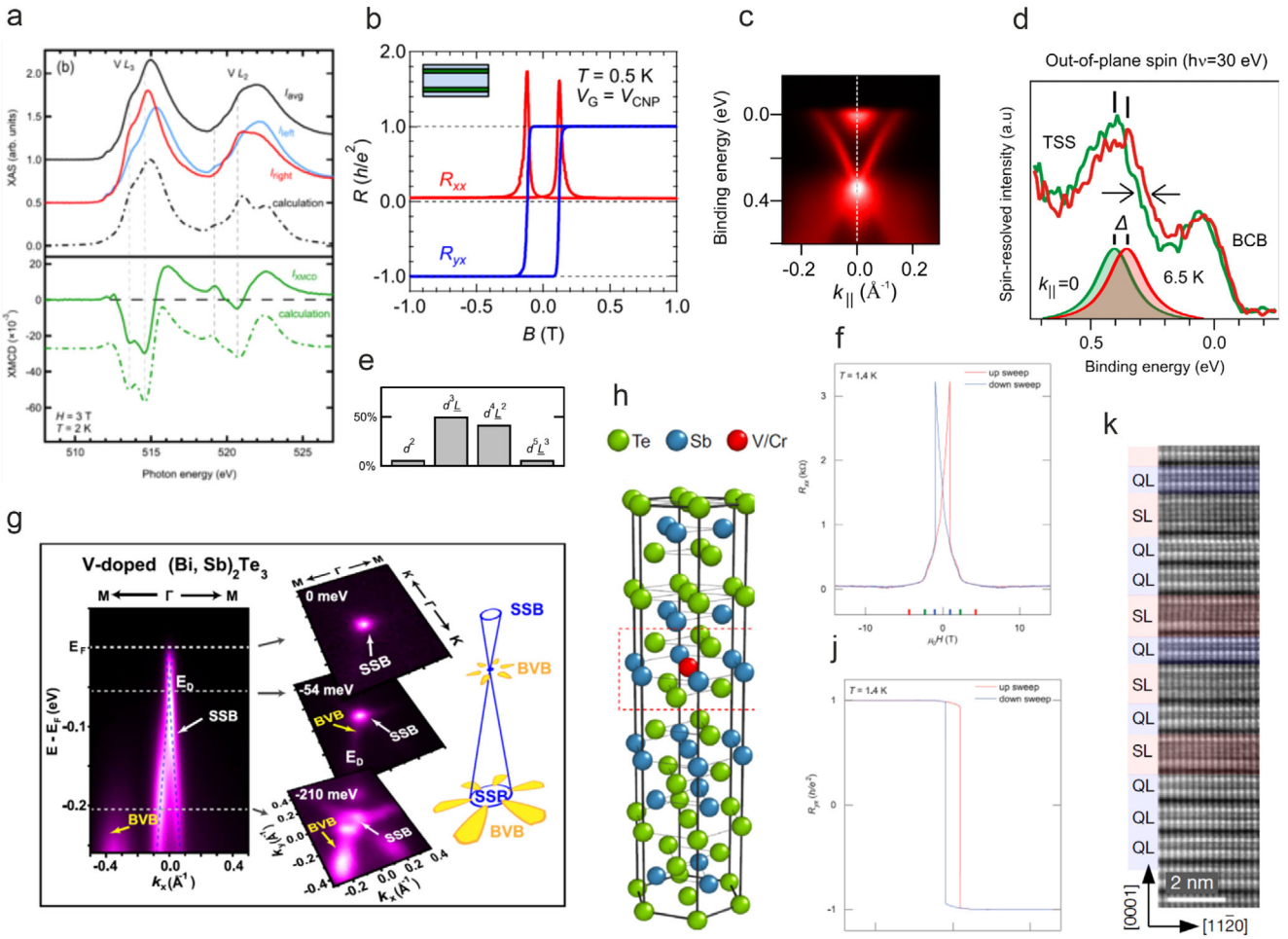

Figure 8. Quantum anomalous Hall (QAH) effect with ferromagnetic topological insulators. Left: random substituted magnetic topological insulators. a) X-ray magnetic circular dichroism of V-doped $(Bi,Sb)_2Te_3$. e) Contributions of different configurations to the ground state. h) Crystal structure of V/Cr-doped Sb_2Te_3 consisting of stacked quintuple layers. Reproduced with permission.[112] Copyright 2020, American Physical Society. b) QAH plateaus of Cr-doped $(Bi,Sb)_2Te_3$ showing the advantage of modulation doping of Cr. The sample consists of 5 layers of which only the green layers are Cr doped. Reproduced with permission.[117] Copyright 2015, AIP Publishing. g) ARPES showing the topological surface state and bulk states possibly degenerate with the magnetic gap which may be detrimental to operation at elevated temperature. Reproduced under the terms of CC BY 4.0 license.[114] Copyright 2016, Springer Nature Right: stoichiometric magnetic topological insulators. c) ARPES of the stoichiometric heterostructure $MnBi_2Te_4/Bi_2Te_3$. d) Spin resolution shows the opening of the magnetic gap of the topological surface state at the Dirac point. k) Transmission electron microscopy of a $MnBi_2Te_4/Bi_2Te_3$ heterostructure. Reproduced with permission.[115] Copyright 2019, Springer Nature. f,j) QAH plateaus of 5 septuple layers $MnBi_2Te_4$. Reproduced with permission.[116] Copyright 2020, American Association for the Advancement of Science.

mechanically exfoliated $MnBi_2Te_4$ the QAH effect occurs up to 1.4 K without and up to 6.5 K with a small applied magnetic field.[116]

Moreover, the QAH effect has recently been observed in stacked 2D materials with moiré structure due to orbital ferromagnetism: in twisted bilayer graphene,[118,119] ABC-stacked trilayer graphene on hBN,[120] and $MoTe_2/WSe_2$ moiré bilayers.[121] The properties of twisted bilayer graphene and the occurrence of the QAH effect[118,119] depend critically on the twist angle. Spatially resolved ARPES[24] is instrumental in determining the flat-band formation which underlies the emergence of orbital ferromagnetism.

4. Optical Quantum Devices

Optical quantum devices harness the quantum properties of light and matter for various applications. Similar defects to the ones employed for qubits can be used but in contrast to the example of P in Si mentioned above, deep in-gap states in large-gap materials are preferred where the transmission of photons is high. The weak interaction of optical photons with the environment leads to large coherence times enabling quantum communications applications. The light can read out specific quantum states within the solid to perform tasks such as sensing magnetic fields with unprecedented sensitivity.

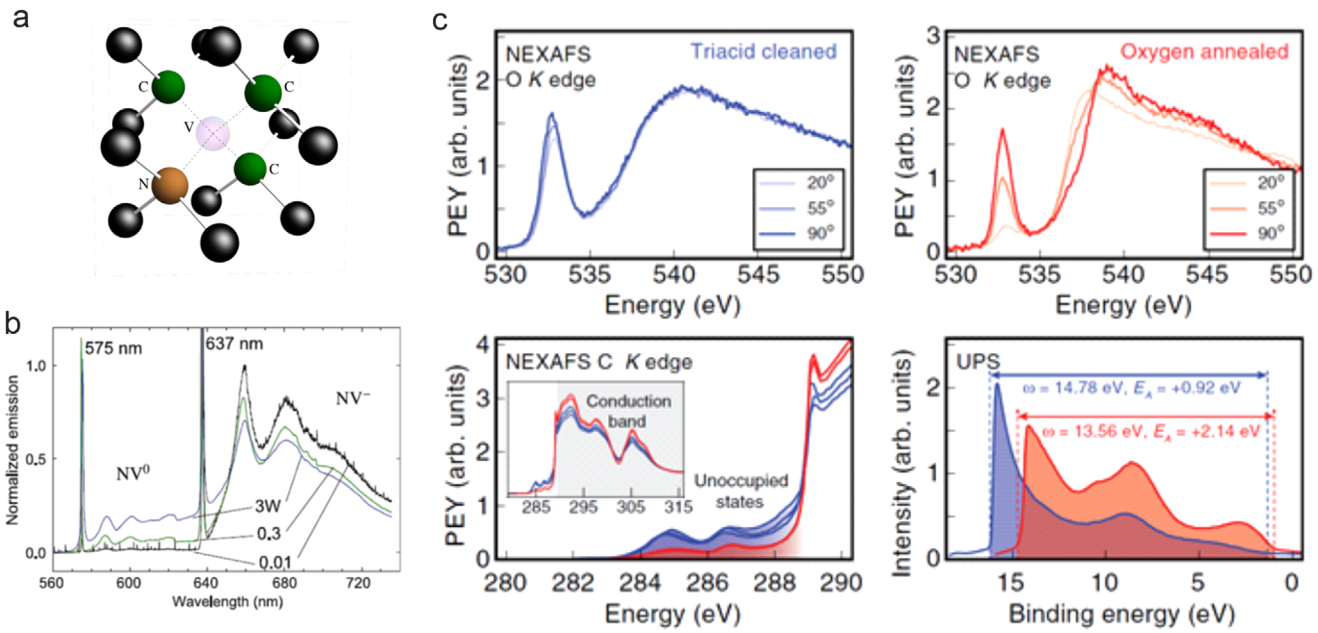

Figure 9. Nitrogen-vacancy (NV) centers for quantum sensing. a) Schematic of the NV center and diamond lattice depicting the vacancy (transparent), the nearest neighbor carbon atoms to the vacancy (green), the substitutional nitrogen atom (brown), and the next-to-nearest carbon neighbors to the vacancy (black). Reproduced with permission.[127] Copyright 2013, Elsevier. b) Normalized emission spectra of an ensemble of NV^- and NV^0 centers at 10 K for different excitation (532 nm) powers as indicated. Reproduced with permission.[128] Copyright 2005, Elsevier. c) Different surface treatments of diamond are compared by oxygen K-edge NEXAFS: blue for triacid cleaned and red for oxygen annealed. The light polarization dependence gives access to the degree of order of the oxygen species in the near-surface region. Reproduced under the terms of CC BY 4.0 license.[125] Copyright 2019, American Physical Society.

4.1. Quantum Sensing

Nitrogen NV centers in diamond constitute a platform for quantum sensing as well as quantum communication and cryptography.[122] In magnetometry, a sub-picotesla sensitivity for dc fields has been reached.[123] If the NV center is near the surface, it can serve as a sensor with subnanometer resolution.[124] However, near the surface, the NV centers are subject to noise from defects at the surface. One problem is that a perfect diamond surface is difficult to achieve due its hardness. An improvement has been achieved with the help of lab-based Ultraviolet Photoelectron Spectroscopy (UPS) and XPS and carbon and oxygen K-edge NEXAFS with synchrotron radiation.[125]

NEXAFS probes the density of unoccupied states near the surface, UPS gives the Fermi energy and electron affinity, and XPS provides information about the chemical state of the surface termination.[125] The oxygen NEXAFS in **Figure 9**c shows a strong dependence on the light polarization indicating well ordered oxygen species at the surface.[125] The carbon NEXAFS in Figure 9c shows independently of the surface treatment (blue for triacid cleaned and red for oxygen annealed) extra peaks, one at 285 eV that is assigned to sp^2 carbon, and one at 286.5 eV assigned to oxygen termination.[126] However, the triacid-cleaned surface shows a 2.4 times higher density of unoccupied states below the conduction band edge, potentially acting as electronic traps that contribute to magnetic and electric field noise.[125] With the help of the surface-science synchrotron-radiation techniques, it was possible to improve the coherence of near-surface NV centers but they remain far from typical bulk values.

Defect levels, such as NV centers in diamond (and VV^0 centers in SiC) are sensitive to local charge as well as magnetism, crystal symmetry and strain which affect the performance of the spin defect.[129] Stroboscopic scanning XRD microscopy was employed for real-space imaging of dynamic strain used in correlation with microscopic photoluminescence measurements.[130] Using nano-focused X-ray photon pulses synchronized to a surface acoustic wave launcher, an effective time resolution of 100 ps was achieved at a 25 nm spatial resolution.[130] In 4H-SiC, excited levels of the neutral VV^0 defect can be manipulated and split with small crystalline strain ($< 10^{-6}$).[131] The acoustically induced local lattice distortions were correlated with enhanced photoluminescence responses of optically active 4H-SiC quantum defects driven by local piezoelectric effects.[130]

In the framework of deterministic synthesis of spin defects in large-bandgap materials,[129] focused ion beam nano-implantation has been combined with strain.sensitive X-ray imaging on the nanoscale (≤ 25 nm).[132] A tensile nano-implanted core was found surrounded by a compressively compensating bulk with peak local strains of about 10^{-5} to $2 \cdot 10^{-4}$. Annealing reduces both the tensile and compressive strain components by an order of magnitude.[132] An increasing number of high-temperature superconductors has been discovered at very high pressures (of the order of Mbar), where tiny (about micron sized) samples are compressed in between the tips of two diamond anvils. A reliable and reproducible characterization of the signatures of superconductivity at such extreme conditions has

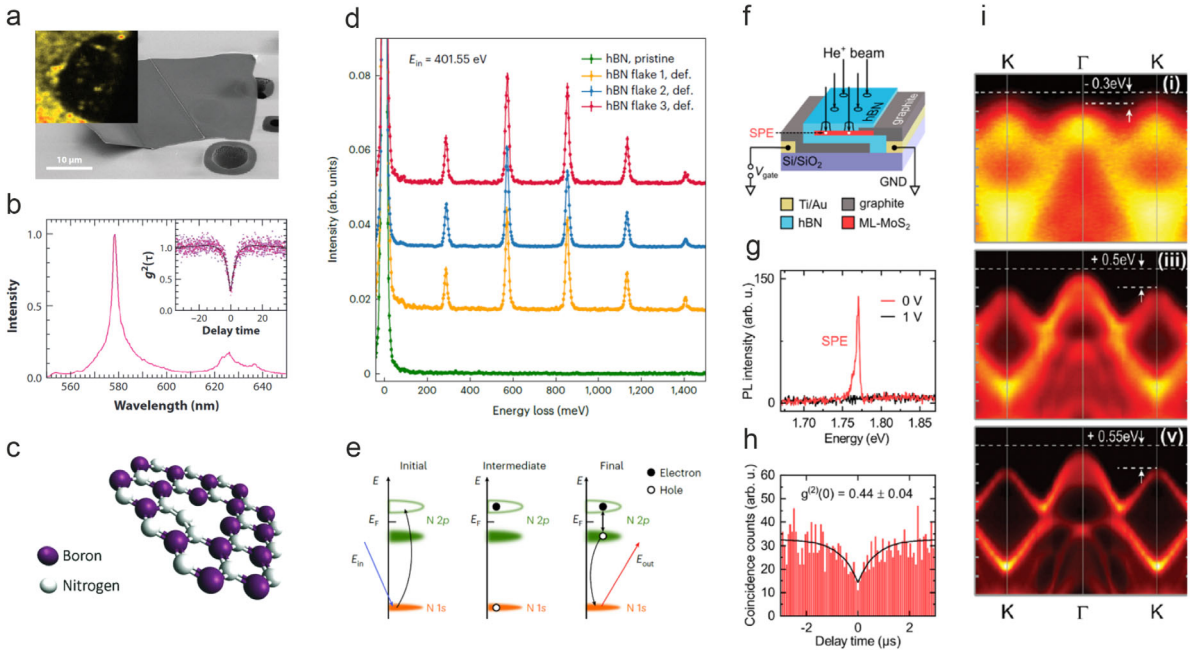

Figure 10. Quantum emitters. a) Secondary-electron microscopy image of a hBN flake with single photon emitters (inset). Reproduced with permission.[150] Copyright 2017, American Chemical Society. b) Photoluminescence and second-order autocorrelation function. c) Schematic illustration of the nitrogen-antisite vacancy center, N_BV_N. Reproduced with permission.[151] Copyright 2018, The Royal Society of Chemistry. d) Resonant inelastic X-ray scattering (RIXS) of hBN with single photon emitters as compared to pristine hBN (green). e) Diagram of the generalized RIXS process at the N–K edge. Reproduced with permission.[146] Copyright 2024, Springer Nature. f, g,h) Gate-switchable arrays of single-photon emitters in a contacted MoS_2 monolayer device. Reproduced with permission.[152] Copyright 2021, American Chemical Society. i) Switching from direct to indirect gap with the thickness in MoS_2 revealed by ARPES with micrometer resolution. Reproduced with permission.[148] Copyright 2016, American Chemical Society.

proved to be difficult, leading to many controversial results (see, e. g. ref. [133]).

NV centers act as sensors because their energy levels and the associated spectra are sensitive to strain and magnetic fields. NV microsensing during high pressure synthesis can in principle be easily combined with synchrotron-radiation XRD to correlate the magnetic or superconducting properties with a well-defined crystallographic structure. Therefore, this method holds great promise to shed light on the controversies in this field of research. Although there have been advances in recent years, the combination of NV magnetometry and XRD to unambiguously characterize both the atomic structure and the superconducting nature of a sample subject to megabar pressures has not yet been reported. One of the challenges that until recently prohibited the application of this method at megabar pressures was the existence of stress in the diamond anvil, which reduces the intensity of the magnetic response of NV centers localized at the anvil tip, setting an effective limit of about half a megabar to the applicability range of these sensors. This has now been solved using different approaches, with the demonstration that it is possible to use NV centers above the megabar and for the moment without a set pressure limit.[134–136]

4.2. Quantum Communication and Cryptography

Quantum communication involves several aspects of communication tasks with the help of quantum mechanics such as quantum teleportation and quantum networking. An important part is quantum cryptography.[137] Quantum key distribution is the most established and practically implemented aspect of quantum cryptography. It provides a way for two parties to generate a shared, random secret key that can be used for encrypting and decrypting messages. A central feature of quantum key distribution is its ability to detect any attempt of eavesdropping. An eavesdropper's interference with the quantum states used in key distribution introduces detectable anomalies. Deterministic single-photon sources will probably be of relevance in advanced quantum key distribution protocols offering ultimate security. Device-independent quantum key distribution[138] is one such protocol and requires very efficient sources of highly indistinguishable photons for entanglement generation.[139]

An important source of single photons are diamond NV centers which we addressed in Section 4.1. Practical difficulties such as with growth and lithographic structuring lead to the exploration of alternative materials. Recently, bright quantum emitters stable at room temperature[140,141] and up to 800 K[142] have been discovered in hBN. **Figure 10b** shows for hBN the photoluminescence and the second-order correlation function, $g^2(\tau)$, which correlates arrival times of photons that reach a detector. The signature of a single-photon emitter is a characteristic dip in $g^2(\tau)$. The relevant defects in hBN are still under debate but one model is N_BV_N, i. e., one N substituting B and a vacancy at the N site.[143] These defects are also promising for the development of 2D quantum sensing units. Magnetic imaging with

hBN flakes and negative boron-vacancy centers has already been demonstrated.[144]

RIXS is a powerful bulk-sensitive technique to determine the low-energy charge, spin, orbital, and lattice excitations of solids.[11] In quantum materials, the entanglement of different degrees of freedom is of particular interest. Recently, the dependence on strain in RIXS measurements has been applied as a tool to reveal this entanglement for the example of Sr_2IrO_4.[145]

Recently, defective hBN has been characterized versus the pristine hBN by RIXS, see Figure 10d,e.[146] Measurements performed at the π^* antibonding orbitals of nitrogen reveal a fundamental excitation E_0 at 285 meV that generates harmonics with energy $E_n = nE_0$ ($n = 1,2, 3,...$) ranging from the mid-infrared up to at least 2.5 eV. The correlation between the harmonics in RIXS and donor-acceptor-pair recombination transitions in photoluminescence indicate that most of the quantum emitters in the hBN have a common origin in the N π^* orbitals.

A second type of single-photon emitters in layered materials are bound excitons that are confined to zero dimensions in a quantum dot due to local strain or a defect. A free exciton can be excited which is then trapped by the quantum dot. Excitons are common in transition-metal dichalcogenides. Here, the interest is due to the fact that they form direct band gaps as monolayers,[147] a property that can be verified directly by ARPES, see Figure 10i (1 to 3 monolayers of WSe_2). By spatially-resolved ARPES, the position of the valence band maxima in the Brillouin zone and (after alkali metal doping) of the conduction band minima have been determined for MoS_2, WS_2, and WSe_2.[148] It is seen in Figure 10i that in MoS_2 the valence band maximum switches from K to Γ when the thickness increases from monolayer to bilayer.[148] Similarly, in ReS_2, a direct gap in the monolayer and bilayer becomes an indirect gap in the bulk.[149] Spin resolution in ARPES is important for these high-spin-orbit materials to identify the interplay of charge, spin and orbital degrees of freedom.[7]

4.3. Quantum Optics in the X-ray Range

There is a broad research field at the intersection of quantum optics and synchrotron radiation. A key ingredient in quantum optics is coherence, which we discussed already above in the context of quantum control in the THz range and for X-ray imaging. Another important aspect is the control of field modes. In visible light, the control of orbital angular momentum is advanced and promises use in classical and quantum communication.[153] Orbital-angular-momentum control has been proposed for undulator radiation in the X-ray range in 2008[154] and was demonstrated for soft X-rays, see **Figure 11a**.[155] One of its advantages will in the future be to access so far forbidden transitions in spectroscopy, for example between *s* and *d* orbitals. Orbital angular momentum is also relevant for entanglement since photon pairs generated by parametric down-conversion are entangled in orbital angular momentum.[156]

The narrow linewidths of nuclear resonances are ideal for transferring concepts of quantum optics to the X-ray range, in particular if one embeds the nuclei in an X-ray cavity.[161] The nuclear transition of lowest excitation energy is the first excited isometric state of ^{229}Th and falls in the vacuum ultraviolet range typically covered by synchrotron radiation and high-harmonic generation lasers. It has been determined as 8.28 eV and allows the nuclear excitation by lasers.[162] This may enable the development of a nuclear optical clock of unprecedented accuracy with an estimated linewidth of $E/\Delta E \approx 10^{20}$ for relativistic geodesy, dark matter research, and the observation of potential temporal variations of fundamental constants.[162]

Another aspect of quantum optics transferred to X-ray energies is nonlinear optics. Parametric down-conversion has been demonstrated early on with X-ray tubes,[163] and the availability of ultrashort brilliant X-ray pulses at FELs has boosted the field and enabled the demonstration and use of further nonlinear effects.[157,158,161,164] Parametric down-conversion is an important source for entangled photons in the visible range and enables entangled X-ray photons as well[158] but the coincidence count rates are very low and only phase matching has been demonstrated so far with the proof of quantum entanglement still outstanding.[161] However, ghost imaging with photon pairs from parametric down-conversion, demonstrated at first for visible light,[165] has been performed with X-ray photon pairs.[166] The experiment, which imaged the widths of two different slits, made use of the insight that the width of the measured parametric down-conversion spectrum is proportional to the width of the used slit.[166] Quantum-enhanced X-ray imaging has been demonstrated recently.[167] Strong quantum correlations between photons generated by X-ray parametric down-conversion were used to enhance image contrast, even in the presence of noise exceeding the signal by several orders of magnitude. Similar approaches could benefit other X-ray-based research, such as studying material defects or determining biomolecular structures.

X-ray second harmonic generation was theoretically proposed in 2003[168] and demonstrated in 2014.[160] At the SACLA X-ray FEL, a pump beam at 7.3 keV was used to generate a second harmonic at 14.6 keV. Phase matching was achieved by using the reciprocal lattice vector normal to the (220) lattice planes of diamond.[160,161] Mixing of X-ray and optical waves has been demonstrated with 8 keV X-ray and 1.5 eV laser pulses[169] as well as in the vacuum ultraviolet range (with 44.9 and 3.1 eV pulses).[159]

5. Quantum Computing for Synchrotron Radiation

While the sections above demonstrate that synchrotron radiation is instrumental for the advancement of quantum technology, one of its core components—quantum computing—holds significant potential to enable new paradigms in data analysis, simulation, and control within synchrotron-radiation and FEL facilities.

This has recently been considered in high-energy physics where quantum computing is a perspective for nonperturbative many-body real-time simulations of lattice gauge theories, for the extraction of rare signals from background events, and for the reconstruction of particle trajectories.[170] Quantum algorithms and quantum simulations[171] could aid in optimizing accelerator operations, potentially improving beam optimisation, control, and other computationally expensive processes.

Quantum computing applied to synchrotron and FEL science will accelerate scientific discovery at these facilities, and will be particularly relevant to high-throughput photon sources, such as diffraction-limited storage rings and high-repetition FELs, which

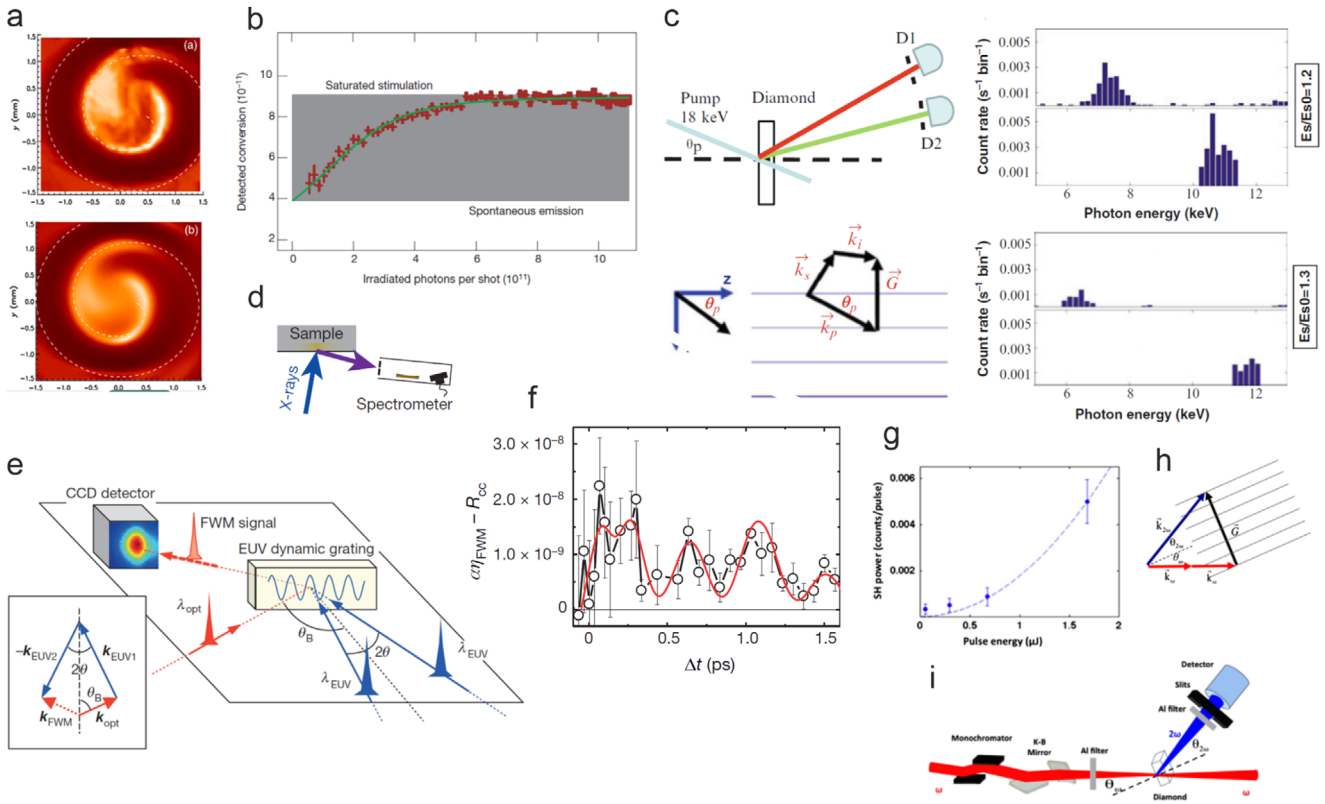

Figure 11. Quantum optical control in the X-ray range. a) Orbital-angular-momentum beam as emitted from an elliptical undulator at BESSY at 99 eV. Reproduced with permission.[155] Copyright 2013, American Physical Society. b,d) Stimulated soft-x-ray emission at 115 eV from FLASH. Reproduced with permission.[157] Copyright 2013, Springer Nature. c) Parametric down-conversion with 18 keV pump photons from SSRL. Reproduced with permission.[158] Copyright 2012, American Physical Society. e,f) Four-wave mixing of vacuum ultraviolet pulses of 44.9 eV at FERMI creating a transient optical grating interacting with 3.15 eV photons. Reproduced with permission.[159] Copyright 2015, Springer Nature. g,h,i) Second-harmonic generation (7.3 and 14.6 keV) at SACLA. Reproduced with permission.[160] Copyright 2014, American Physical Society.

presently can exceed 1 petabyte of data collected per day, and which rely on real-time information to optimally steer experiments. In this case, quantum computing could expedite certain tasks such as the identification of the scientifically valuable fraction of collected data, or the interpretation of the outcomes of an experiment, with transformative implications with respect to the quality and quantity of scientific results and the time to achieve them. By using such methods on data offline, new strategies could be developed to evaluate the data quality amongst collected datasets. With such information, more robust data reduction methods could be developed to tackle the large data volumes produced, thereby increasing the data quality density.

Among data-intensive techniques that could be transformed by quantum computing are XRF, coherent diffraction imaging, STXM, NEXAFS, and X-ray tomography, which already have emerging quantum computing counterparts.[172]

For instance, quantum computing could significantly enhance the processing and interpretation of complex spectral data in XRF, where it can rapidly analyze element-specific signals across varying oxidation states. In coherent diffraction imaging, quantum-computing-powered simulations could facilitate high-resolution 3D imaging reconstructions, providing detailed structural insights into materials without iterative data refinement. In STXM and NEXAFS, the ability of quantum computing to simulate electronic structures could lead to more precise analyses of molecular and electronic configurations. Quantum computing could also accelerate tomographic reconstructions, enabling faster imaging and real-time applications in dynamic systems or high-throughput experiments. Existing quantum-computing algorithms such as for optimisation like the Quantum Approximate Optimization Algorithm (QAOA),[173] searching,[174] and (quantum) Fourier transformations,[175] are already implementable in commercially available systems, albeit with known limitations. Classical implementations of these algorithms are essential computational elements for many synchrotron-radiation techniques—including computer X-ray tomography, STXM, and XRF—thus their quantum computing equivalents have direct application potential.

Beyond core mathematical operations like those mentioned above, broader quantum computing fields are applicable to synchrotron-radiation research. Notably the interdisciplinary field of quantum machine learning at the intersection of quantum computing and machine learning inherits the applicability of the latter in synchrotron radiation.[176,177] Machine learning significantly impacts synchrotron facilities, having demonstrated beam stabilization through feed-forward correction using neural networks,[178] improved daily beamline operations, enhanced applications in X-ray absorption,

scattering, and photoemission,[179,180] facilitated quantum-material discovery,[181] accelerated multimodal scanning strategies,[182] and automated experimentation via feedback loops.[183] Similarly, machine learning has been applied across a range of areas at X-ray FEL facilities, including online data analysis and signal extraction,[184] the detection of phase transitions,[185] and virtual diagnostics aimed at improving data quality and enabling automated calibration.[186]

The integration of machine learning with quantum computing may offer further advantages, combining the processing power of quantum computing with the capacity of artificial intelligence for pattern recognition and data extraction as shown in new outcomes from quantum machine learning.[176,177,187] Early results of significance exist for quantum material simulation[188,189] suggesting higher accuracy compared to machine learning methods. Hybrid classical-quantum or pure quantum computing strategies could lead to new approaches in data management and interpretation, automating tasks like peak fitting, noise reduction, and the real-time correlation of experimental parameters across large datasets such as those used in ptychography and coherent diffraction imaging. Ultimately, the convergence of quantum computing, artificial intelligence, and synchrotron radiation techniques could significantly benefit the field,[170] enhancing precision, efficiency, and breadth of insight across materials science, biology, and beyond. Last but not least such progress may further increase the impact that synchrotron-radiation facilities have in the advancement of quantum technologies.

Although quantum computing is at its early stages and progress assumes the advent of large-scale, fault-tolerant devices, new research exhibits results even with a single ancillary qubit for state tomography for quantum simulation and computation of scattering amplitudes.[190] Encouraged by these advancements and their potential, synchrotron-radiation facilities—including Elettra, DESY, SLAC, and BNL—have taken strategic early steps by establishing dedicated quantum computing divisions. Investing in this research now is essential to building critical mass in the field, ensuring that facilities are well positioned to lead when the technology reaches greater maturity.

6. Outlook

Materials and their interfaces enable quantum technologies, and synchrotron- and FELradiation techniques offer the possibility to better understand materials and interfaces and thus rationally optimize their performance. We therefore expect the significance of materials science for quantum technology to increase and synchrotron and FEL radiation to play an increasingly important role.

As a relevant example, superconducting qubits illustrate this point. We have mentioned above the advantages of Ta for superconducting qubits due to its stoichiometric oxide and the help of depth profiling by XPS with synchrotron radiation. According to ref. [1], there are about 20 more candidate materials already today waiting to be explored, among them TiN and NbTiN. More collaboration across fields can be expected. As an example, superconducting radio frequency accelerators in FELs suffer from dielectric loss due to oxides as well.

It has to be investigated which surface or interface affects T_2. Due to the ultralow operating temperatures of superconducting qubits, this cannot be done in operando. On the other hand, it is important to study the effects of temperature and power cycling. It has been pointed out that coherence times and gate fidelities are useful parameters in assessing smaller units but do not capture the requirements for operation of large-scale systems.[1] Hence, coping with upscaling to a large number of qubits will be a task for research involving testing, e.g., for variations in performance.

Besides the mentioned two-level systems in dielectrics, the performance of superconducting qubits is also limited by loss and dissipation due to quasiparticle excitations from broken Cooper pairs.[1] It has recently been achieved to measure an extremely low pair breaking rate of 1.5 Hz.[191] The experiment rules out commonly suggested origins such as insufficient shielding against stray light or ionizing radiation but the origin and dynamics are still unclear.[191]

For Si quantum dots, a future application of strain concerns the question of enhanced valley splitting by shear strain. The valley splitting in Si will be particularly important for system sizes beyond two qubits.[192] It has been predicted that shear strain will enhance the splitting but the experimental confirmation is still outstanding.[193] Insight into the structure around defects and characterization of electronic states in the near surface region (down to 3 nm) is demanded. This may also require multimodal experiments from THz to X-rays and the combination of ion irradiation and implantation facilities with synchrotron-radiation methods. Synchrotron-radiation methods will also continue to explore new lithography methods, such as extreme ultraviolet (EUV) lithography using partially H-terminated Si.[194] It is expected that a resistless EUV lithography method offers a promising route to nanometer-scale patterning by eliminating the resolution and roughness constraints associated with conventional photoresist materials.

In general, we are poised to observe an expansion of the materials spectrum for quantum technologies, encompassing conventional semiconductors and superconductors as well as quantum materials. The strong property-function correlation inherent in quantum materials will become increasingly important. The topological superconductor has still to be identified where ARPES at low temperatures plays an important role. An assessment of novel materials from an applied and electrical engineering perspective is necessary.[195] Benchmarking of established topological materials such as Bi_2Se_3 and Bi_2Te_3 versus CMOS materials for applications such as topological versions of the field effect transistor, p-n-junctions, interconnects, and spin-orbit torque has recently been undertaken.[195]

In particular in quantum sensing and quantum communication, it appears that layered quantum materials, here 2D materials, are rapidly surpassing classical materials, here covalently bonded 3D semiconductors, in performance. This can be seen in color centers in hBN versus those in diamond. It has been pointed out that it took less than three years from optical to electrical excitation of quantum emitters in transition-metal dichalcogenides and less than two years from the identification of localized spins in hBN to coherent control.[5]

While we have seen in the above the importance of strain and its analysis by synchrotron radiation methods for conventional materials in quantum technology, its importance for 2D layered

materials is even greater.[196] Strain control allows spectral tunability of single photon emitters in a 100 nm thick hBN flake over 6 meV.[141] This is crucial for reaching spectral overlap among different emitters. It was found that the achieved strain and pressure tuning as well as Stark shift tuning in hBN are larger by almost an order of magnitude than for defects in 3D systems such as diamond.[143]

Recently, the G-center in Si has emerged as a promising spin qubit candidate which, on the one hand, integrates in existing Si platforms and, on the other hand, is also a single-photon emitter in the telecommunications O-band. The defect consists of two substitutional carbon atoms connected by an interstitial Si atom and can be individually addressed.[197] The defect has been identified as bistable[198] which poses a particular challenge for structural investigations.

In operando methods will play an important role. This relates to established sample environments such as high magnetic fields but also electric fields, gating, current, and strain. Spatial resolution is important to distinguish the effects of the external stimuli, e.g., in in-operando ARPES.[24]

The field will benefit from further development of nano-focused coherent diffraction imaging techniques and the potential to image time-varying acoustic strain at sub-10 nm 3D resolution near far-from-surface lattice defects.[130] The tilted geometry of laminography allows to make additional use of the stronger interaction of soft X-rays with matter, using contrast based on chemical sensitivity, oxidation states, and magnetic dichroism.[199] As more diffraction-limited storage-ring light sources come into operation, their higher coherent fraction will enable these experiments on a regular basis. It can be expected that synchrotron radiation will not only be used in research and development but also in quality control, requiring installations for high-throughput techniques.

Finally, we can expect that FELs and X-ray FELs will play an increasingly important role in the years to come, by providing unique opportunities to probe ultrafast dynamics in quantum materials and to develop new quantum-optics-based methods in the X-ray regime.

A revolutionary breakthrough in the application of X-ray FEL radiation in the field of quantum technologies can be expected with the onset of operation of X-ray free electron laser oscillators (XFELO). These promise to deliver fully coherent X-ray FEL pulses, with spatial and temporal coherence similar to optical lasers.[200,201] Such sources will represent a new paradigm for X-ray FEL radiation with outstanding radiation characteristics: orders of magnitude higher peak spectral flux than self-amplified spontaneous emission (SASE) and higher shot to shot stability than self-seeding. In a self-seeding scheme, the SASE FEL radiation generated in the first part of an FEL undulator is monochromatized and subsequently amplified to its final properties in the second part. This allows to increase the peak brightness of SASE X-ray pulses and decrease their spectral bandwidth, thereby leading to enhanced temporal coherence.[202–204]

Already today, hard X-ray self-seeding has led to unprecedented spectral brilliance (approximately 10-fold increase with respect to SASE), enabling for the first time the detection of the 1.4 femto-eV linewidth of the nuclear isotope ^{45}Sc.[205] XFELO radiation will provide an additional approximately tenfold or more increase in spectral brilliance, boosting the cross section for excitation of extremely narrow nuclear resonances and giving routine access to a large variety of methods for transferring concepts of quantum optics to the X-ray range. An example of immediate application will be the proof of quantum entanglement in the x-ray regime by parametric down-conversion: all attempts so far have failed because coincidence count rates are too low.

Other applications likely to be revolutionized by XFELOs are those utilizing ultra-fast spectroscopies at meV energy resolution and necessitating very high signal-to-noise ratio to detect the dynamics of tiny changes in spin, electronic or vibrational degrees of freedom. Examples are the detection of entanglement of different degrees of freedom in highly correlated electron systems by RIXS, phonon dispersion in qubit molecules by IXS or the investigation of the correlation between intramolecular vibrations (by IXS) and spin relaxation (by spin resolved ARPES) in crystals. We can anticipate that many other open science questions, many of them inspired by examples illustrated in this article, will find answers through the routine deployment of XFELOs in the coming decade.

Acknowledgements

The present article was partially based on the conference "LEAPS meets quantum technology" (Elba, 2022) funded by LEAPS, the League of European Accelerator-based Photon Sources, and the authors thank participants and organizers, in particular Massimo Ferrario and Søren Pape-Møller. The authors were grateful to Zakaria Dahbi, Paul G. Evans, Simon Gerber, Megan O. Hill, Matthieu Le Tacon, Nathalie de Leon, Ben Murdin, Jean-François Roch, Sharon Shwartz, Vladimir Strocov, Sangeeta Thakur, and Balu Thiagarajan for helpful discussions. O. R., A. A. M., and K. T. acknowledged LEAPS-INNOV WP9, funded from the European Union Horizon 2020 programme under grant agreement no. 101004728. The work also received funding from the European Union–NextGenerationEU, PNRR MUR Project PE0000023-NQSTI. [Correction added on November 19, 2025, after first online publication: Some minor corrections have been added in this version.]

Open access funding enabled and organized by Projekt DEAL.

Conflict of Interest

The authors declare no conflict of interest.

Keywords

decoherence, depth profiling, impurities, quantum computing, quantum sensing, quantum metrology, strain

Received: January 12, 2025
Revised: September 12, 2025
Published online: October 22, 2025

[1] N. P. de Leon, K. M. Itoh, D. Kim, K. K. Mehta, T. E. Northup, H. Paik, B. S. Palmer, N. Samarth, S. Sangtawesin, D. W. Steuerman, *Science* **2021**, *372*, eabb2823.
[2] V. Lordi, J. M. Nichol, *MRS Bull.* **2021**, *46*, 589.
[3] C. E. Murray, *Mater. Sci. Eng.: R: Rep.* **2021**, *146*, 100646.
[4] X. Liu, M. C. Hersam, *Nat. Rev. Mater.* **2019**, *4*, 669.
[5] A. R.-P. Montblanch, M. Barbone, I. Aharonovich, M. Atatüre, A. C. Ferrari, *Nat. Nanotechnol.* **2023**, *18*, 555.

[6] A. Acín, I. Bloch, H. Buhrman, T. Calarco, C. Eichler, J. Eisert, D. Esteve, N. Gisin, S. J. Glaser, F. Jelezko, S. Kuhr, M. Lewenstein, M. F. Riedel, P. O. Schmidt, R. Thew, A. Wallraff, I. Walmsley, F. K. Wilhelm, *New J. Phys.* **2018**, *20*, 08020.
[7] H. Dosch, *Nat. Rev. Mater.* **2019**, *4*, 459.
[8] R. Abela, C. Biscari, J. Daillant, H. Dosch, L. Rivkin, *Eur. Phys. J. Plus* **2023**, *138*, 355.
[9] X. Yan, D. D. Fong, H. Zhou, J. L. McChesney, *J. Appl. Phys.* **2021**, *129*, 220902.
[10] L. Helfen, T. Baumbach, P. Mikulik, D. Kiel, P. Pernot, P. Cloetens, J. Baruchel, *Appl. Phys. Lett.* **2005**, *86*, 071915.
[11] L. J. P. Ament, M. van Veenendaal, T. P. Devereaux, J. P. Hill, J. van den Brink, *Rev. Mod. Phys.* **2011**, *83*, 705.
[12] P. Kaye, R. Laflamme, M. Mosca, *An introduction to Quantum Computing*, Oxford University Press, Oxford **2010**.
[13] Y. Cao, J. Romero, J. P. Olson, M. Degroote, P. D. Johnson, M. Kieferová, I. D. Kivlichan, T. Menke, B. Peropadre, N. P. D. Sawaya, S. Sim, L. Veis, A. Aspuru-Guzik, *Chem. Rev.* **2019**, *119*, 10856.
[14] G. D. Scholes, *Proc. R. Soc. A* **2023**, *479*, 20230599.
[15] A. Chiesa, P. Santini, E. Garlatti, F. Luis, S. Carretta, *Rep. Prog. Phys.* **2024**, *87*, 034501.
[16] G. D. Scholes, A. Olaya-Castro, S. Mukamel, A. Kirrander, K.-K. Ni, G. J. Hedley, N. L. Frank, *J. Phys. Chem. Lett.* **2025**, *16*, 1376.
[17] P. W. Shor, *SIAM J. Comput.* **1997**, *26*, 1484.
[18] D. P. DiVincenzo, *Fortschr. Phys.* **2000**, *48*, 771.
[19] S. J. Devitt, W. J. Munro, K. Nemoto, *Rep. Prog. Phys.* **2013**, *76*, 076001.
[20] M. Holler, M. Odstrcil, M. Guizar-Sicairos, M. Lebugle, E. Müller, S. Finizio, G. Tinti, C. David, J. Zusman, W. Unglaub, O. Bunk, J. Raabe, A. F. J. Levi, G. Aeppli, *Nat. Electron.* **2019**, *2*, 464.
[21] E. Kröger, A. Petraru, A. Hanff, R. Soni, M. Kalläne, J. D. Denlinger, T. Learmonth, J.-H. Guo, K. E. Smith, T. Schneller, B. Freelon, L. Kipp, H. Kohlstedt, K. Rossnagel, G. Kolhatkar, *Appl. Phys. Lett.* **2022**, *120*, 181601.
[22] E. Rotenberg, In *X-rays in Nanoscience: Spectroscopy, Spectromicroscopy and Scattering Techniques*, (Ed: J. Guo), chapter 6, Wiley-VCH, Weinheim, **2010**, pp. 169–206.
[23] P. V. Nguyen, N. C. Teutsch, N. P. Wilson, J. Kahn, X. Xia, A. J. Graham, V. Kandyba, A. Giampietri, A. Barinov, G. C. Constantinescu, N. Yeung, N. D. M. Hine, X. Xu, D. H. Cobden, N. R. Wilson, *Nature* **2019**, *572*, 220.
[24] P. Hofmann, *AVS Quantum Sci.* **2021**, *3*, 021101.
[25] F. Joucken, J. Avila, Z. Ge, E. A. Quezada-Lopez, H. Yi, R. Le Goff, E. Baudin, J. L. Davenport, K. Watanabe, T. Taniguchi, M. C. Asensio, J. Velasco Jr, *Nano Lett.* **2019**, *19*, 2682.
[26] F. Arute, K. Arya, R. Babbush, D. Bacon, J. C. Bardin, R. Barends, R. Biswas, S. Boixo, F. G. S. L. Brandao, D. A. Buell, B. Burkett, Y. Chen, Z. Chen, B. Chiaro, R. Collins, W. Courtney, A. Dunsworth, E. Farhi, B. Foxen, A. Fowler, C. Gidney, M. Giustina, R. Graff, K. Guerin, S. Habegger, M. P. Harrigan, M. J. Hartmann, A. Ho, M. Hoffmann, T. Huang, et al., *Nature* **2019**, *574*, 505.
[27] A. Wallraff, D. I. Schuster, A. Blais, L. Frunzio, R.-S. Huang, J. Majer, S. Kumar, S. M. Girvin, R. J. Schoelkopf, *Nature* **2004**, *431*, 162.
[28] A. Blais, A. L. Grimsmo, S. M. Girvin, A. Wallraff, *Rev. Mod. Phys.* **2021**, *93*, 025005.
[29] M. Kjaergaard, M. E. Schwartz, J. Braumüller, P. Krantz, J. I.-J. Wang, S. Gustavsson, W. D. Oliver, *Annu. Rev. Condens. Matter Phys.* **2020**, *11*, 369.
[30] R. A. McLellan, A. Dutta, C. Zhou, Y. Jia, C. Weiland, X. Gui, A. P. M. Place, K. D. Crowley, X. H. Le, T. Madhavan, Y. Gang, L. Baker, A. R. Head, I. Waluyo, R. Li, K. Kisslinger, A. Hunt, I. Jarrige, S. A. Lyon, A. M. Barbour, R. J. Cava, A. A. Houck, S. L. Hulbert, M. Liu, A. L. Walter, N. P. de Leon, *Adv. Sci.* **2023**, *10*, 2300921.
[31] J. Koch, T. M. Yu, J. Gambetta, A. A. Houck, D. I. Schuster, J. Majer, A. Blais, M. H. Devoret, S. M. Girvin, R. J. Schoelkopf, *Phys. Rev. A* **2007**, *76*, 042319.
[32] A. P. M. Place, L. V. H. Rodgers, P. Mundada, B. M. Smitham, M. Fitzpatrick, Z. Leng, A. Premkumar, J. Bryon, A. Vrajitoarea, S. Sussman, G. Cheng, T. Madhavan, H. K. Babla, X. H. Le, Y. Gang, B. Jäck, A. Gyenis, N. Yao, R. J. Cava, N. P. de Leon, A. A. Houck, *Nat. Commun.* **2021**, *12*, 1779.
[33] C. Wang, X. Li, H. Xu, Z. Li, J. Wang, Z. Yang, Z. Mi, X. Liang, T. Su, C. Yang, G. Wang, W. Wang, Y. Li, M. Chen, C. Li, K. Linghu, J. Han, Y. Zhang, Y. Feng, Y. Song, T. Ma, J. Zhang, R. Wang, P. Zhao, W. Liu, G. Xue, Y. Jin, H. Yu, *npj Quantum Inf.* **2022**, *8*, 1.
[34] D. P. Lozano, M. Mongillo, X. Piao, S. Couet, D. Wan, Y. Canvel, A. M. Vadiraj, T. Ivanov, J. Verjauw, R. Acharya, J. Van Damme, F. A. Mohiyaddin, J. Jussot, P. P. Gowda, A. Pacco, B. Raes, J. Van de Vondel, I. P. Radu, B. Govoreanu, J. Swerts, A. Potočnik, K. De Greve, *Adv. Sci.* **2025**, e09244.
[35] A. Premkumar, C. Weiland, S. Hwang, B. Jäck, A. P. M. Place, I. Waluyo, A. Hunt, V. Bisogni, J. Pelliciari, A. Barbour, M. S. Miller, P. Russo, F. Camino, K. Kisslinger, X. Tong, M. S. Hybertsen, A. A. Houck, I. Jarrige, *Commun. Mater.* **2021**, *2*, 72.
[36] K. D. Crowley, R. A. McLellan, A. Dutta, N. Shumiya, A. P. M. Place, X. H. Le, Y. Gang, T. Madhavan, N. Khedkar, Y. C. Feng, E. A. Umbarkar, X. Gui, L. V. H. Rodgers, Y. Jia, M. M. Feldman, S. A. Lyon, M. Liu, R. J. Cava, A. A. Houck, N. P. de Leon, *Phys. Rev. X* **2023**, *13*, 041005.
[37] G. Burkard, T. D. Ladd, A. Pan, J. M. Nichol, J. R. Petta, *Rev. Mod. Phys.* **2023**, *95*, 025003.
[38] D. Loss, D. P. DiVincenzo, *Phys. Rev. A* **1998**, *57*, 120.
[39] J. R. Petta, A. C. Johnson, J. M. Taylor, E. A. Laird, A. Yacoby, M. D. Lukin, C. M. Marcus, M. P. Hanson, A. C. Gossard, *Science* **2005**, *309*, 2180.
[40] K. C. Nowack, M. Shafiei, M. Laforest, G. E. D. K. Prawiroatmodjo, L. R. Schreiber, C. Reichl, W. Wegscheider, L. M. K. Vandersypen, *Science* **2011**, *333*, 1269.
[41] J. P. Dodson, N. Holman, B. Thorgrimsson, S. F. Neyens, E. R. MacQuarrie, T. McJunkin, R. H. Foote, L. F. Edge, S. N. Coppersmith, M. A. Eriksson, *Nanotechnology* **2020**, *31*, 505001.
[42] M. Veldhorst, C. H. Yang, J. C. C. Hwang, W. Huang, J. P. Dehollain, J. T. Muhonen, S. Simmons, A. Laucht, F. E. Hudson, K. M. Itoh, A. Morello, A. S. Dzurak, *Nature* **2015**, *526*, 410.
[43] E. J. Connors, J. Nelson, H. Qiao, L. F. Edge, J. M. Nichol, *Phys. Rev. B* **2019**, *100*, 165305.
[44] B. E. Kane, *Nature* **1998**, *393*, 133.
[45] J. Muhonen, J. Dehollain, A. Laucht, F. Hudson, T. Sekiguchi, K. Itoh, D. Jamieson, J. McCallum, A. Dzurak, A. Morello, *Nat. Nanotechnol.* **2014**, *9*, 986.
[46] K. L. Litvinenko, E. T. Bowyer, P. T. Greenland, N. Stavrias, J. Li, R. Gwilliam, B. J. Villis, G. Matmon, M. L. Y. Pang, B. Redlich, A. F. G. van der Meer, C. R. Pidgeon, G. Aeppli, B. N. Murdin, *Nat. Commun.* **2015**, *6*, 6549.
[47] M. G. Masteghin, T. Gervais, S. K. Clowes, D. C. Cox, V. Zelyk, A. Pattammattel, Y. S. Chu, N. Kolev, T. Z. Stock, N. Curson, P. G. Evans, M. Stuckelberger, B. N. Murdin, *Small Methods* **2024**, 2301610.
[48] A. M. Stoneham, A. J. Fisher, P. T. Greenland, *J. Phys.: Condens. Matter* **2003**, *15*, L447.
[49] K. L. Litvinenko, S. G. Pavlov, H.-W. Hübers, N. V. Abrosimov, C. R. Pidgeon, B. N. Murdin, *Phys. Rev. B* **2014**, *89*, 235204.
[50] K. Saeedi, N. Stavrias, B. Redlich, A. F. G. van der Meer, R. Mikhaylovskiy, A. V. Kimel, C. R. Pidgeon, B. N. Murdin, *J. Phys.: Condens. Matter* **2019**, *31*, 435401.
[51] J. J. Pla, K. Y. Tan, J. P. Dehollain, W. H. Lim, J. J. L. Morton, D. N. Jamieson, A. S. Dzurak, A. Morello, *Nature* **2012**, *489*, 541.

[52] J. C. McCallum, B. C. Johnson, T. Botzem, *Appl. Phys. Rev.* **2021**, *8*, 031314.
[53] M. A. Broome, S. K. Gorman, M. G. House, S. J. Hile, J. G. Keizer, D. Keith, C. D. Hill, T. F. Watson, W. J. Baker, L. C. L. Hollenberg, M. Y. Simmons, *Nat. Commun.* **2018**, *9*, 980.
[54] N. Cassidy, P. Blenkinsopp, I. Brown, R. J. Curry, B. N. Murdin, R. Webb, D. Cox, *Phys. Status Solidi* **2021**, *218*, 2170010.
[55] J. O'Gorman, N. H. Nickerson, P. Ross, J. J. L. Morton, S. C. Benjamin, *npj Quantum Inform.* **2016**, *2*, 15019.
[56] E. Ferraro, D. Rei, M. Paris, M. D Michielis, *EPJ Quantum Technol.* **2022**, *9*, 2.
[57] J. A. Miwa, P. Hofmann, M. Y. Simmons, J. W. Wells, *Phys. Rev. Lett.* **2013**, *110*, 136801.
[58] P. Constantinou, T. J. Z. Stock, E. Crane, A. Kölker, M. van Loon, J. Li, S. Fearn, H. Bornemann, N. D'Anna, A. J. Fisher, V. N. Strocov, G. Aeppli, N. J. Curson, S. R. Schofield, *Adv. Sci.* **2023**, *10*, 2302101.
[59] F. A. Zwanenburg, A. S. Dzurak, A. Morello, M. Y. Simmons, L. C. L. Hollenberg, G. Klimeck, S. Rogge, S. N. Coppersmith, M. A. Eriksson, *Rev. Mod. Phys.* **2013**, *85*, 961.
[60] C. Corley-Wiciak, et al., *Phys. Rev. Appl.* **2023**, *20*, 024056.
[61] A. Pateras, J. Park, Y. Ahn, J. A. T, M. V. Holt, C. Reichl, W. Wegscheider, T. A. Baart, J. P. Dehollain, U. Mukhopadhyay, L. M. K. Vandersypen, P. G. Evans, *Nano Lett.* **2018**, *18*, 2780.
[62] A. Pateras, J. Carnis, U. Mukhopadhyay, M.-I. Richard, S. J. Leake, T. U. Schülli, C. Reichl, W. Wegscheider, J. P. Dehollain, L. M. Vandersypen, P. G. Evans, *J. Mater. Res.* **2019**, *34*, 1291.
[63] C. Corley-Wiciak, C. Richter, M. H. Zoeller, I. Zaitsev, C. L. Manganelli, et al., *ACS Appl. Mater. Interfaces* **2023**, *15*, 3119.
[64] M. Eich, F. Herman, R. Pisoni, H. Overweg, A. Kurzmann, Y. Lee, P. Rickhaus, K. Watanabe, T. Taniguchi, M. Sigrist, T. Ihn, K. Ensslin, *Phys. Rev. X* **2018**, *8*, 031023.
[65] R. Garreis, C. Tong, J. Terle, M. J. Ruckriegel, J. D. Gerber, L. M. Gächter, K. Watanabe, T. Taniguchi, T. Ihn, K. Ensslin, W. W. Huang, *Nat. Phys.* **2024**, *20*, 428.
[66] T. Ohta, A. Bostwick, T. Seyller, K. Horn, E. Rotenberg, *Science* **2006**, *313*, 951.
[67] M. Eich, R. Pisoni, A. Pally, H. Overweg, A. Kurzmann, Y. Lee, P. Rickhaus, K. Watanabe, T. Taniguchi, K. Ensslin, T. Ihn, *Nano Lett.* **2018**, *18*, 5042.
[68] X.-X. Song, D. Liu, V. Mosallanejad, J. You, T.-Y. Han, D.-T. Chen, H.-O. Li, G. Cao, M. Xiao, G.-C. Guo, G.-P. Guo, *Nanoscale* **2015**, *7*, 16867.
[69] A. Y. Kitaev, *Ann. Phys.* **2003**, *303*, 2.
[70] S. Das Sarma, M. Freedman, C. Nayak, *npj Quantum Inform.* **2015**, *1*, 15001.
[71] S. Das Sarma, M. Freedman, C. Nayak, *Phys. Rev. Lett.* **2005**, *94*, 166802.
[72] S. Das Sarma, C. Nayak, S. Tewari, *Phys. Rev. B* **2006**, *73*, 220502(R).
[73] Y. Liu, Z.-Q. Mao, *Physica C* **2015**, *514*, 339.
[74] X.-L. Qi, T. L. Hughes, S.-C. Zhang, *Phys. Rev. B* **2010**, *82*, 184516.
[75] B. Lian, X.-Q. Sun, A. Vaezi, X.-L. Qi, S.-C. Zhang, *Proc. Natl Acad. Sci. USA* **2018**, *115*, 10938.
[76] M. Kayyalha, D. Xiao, R. Zhang, J. Shin, J. Jiang, F. Wang, Y.-F. Zhao, R. Xiao, L. Zhang, K. M. Fijalkowski, P. Mandal, M. Winnerlein, C. Gould, Q. Li, L. W. Molenkamp, M. H. W. Chan, N. Samarth, C.-Z. Chang, *Science* **2020**, *367*, 64.
[77] R. M. Lutchyn, J. D. Sau, S. Das Sarma, *Phys. Rev. Lett.* **2010**, *105*, 077001.
[78] Y. Oreg, G. Refael, F. von Oppen, *Phys. Rev. Lett.* **2010**, *105*, 177002.
[79] V. Mourik, K. Zuo, S. M. Frolov, S. R. Plissard, E. P. A. M. Bakkers, L. P. Kouwenhoven, *Science* **2012**, *336*, 1003.
[80] J. Krieg, C. Chen, J. Avila, Z. Zhang, W. Sigle, H. Zhang, C. Trautmann, M. C. Asensio, M. E. Toimil-Molares, *Nano Lett.* **2016**, *16*, 4001.
[81] P. Corfdir, O. Marquardt, R. B. Lewis, C. Sinito, M. Ramsteiner, A. Trampert, U. Jahn, L. Geelhaar, O. Brandt, V. M. Fomin, *Adv. Mater.* **2019**, *31*, 1805645.
[82] S. R. Plissard, D. R. Slapak, M. A. Verheijen, M. Hocevar, G. W. G. Immink, I. van Weperen, S. Nadj-Perge, S. M. Frolov, L. P. Kouwenhoven, E. P. A. M. Bakkers, *Nano Lett.* **2012**, *12*, 1794.
[83] S. Hammarberg, V. Dagytė, L. Chayanun, M. O. Hill, A. Wyke, A. Björling, U. Johansson, S. Kalbfleisch, M. Heurlin, L. J. Lauhon, M. T. Borgström, J. Wallentin, *Nano Res.* **2020**, *13*, 2460.
[84] S. Hammarberg, D. Dzhigaev, L. A. B. Marçal, V. Dagytė, A. Björling, M. T. Borgström, J. Wallentin, *J. Appl. Crystallogr.* **2024**, *57*, 60.
[85] T. Yu, J. Wright, G. Khalsa, B. Pamuk, C. S. Chang, Y. Matveyev, X. Wang, T. Schmitt, D. Feng, D. A. Muller, H. G. Xing, D. Jena, V. N. Strocov, *Sci. Adv.* **2021**, *7*, eabi5833.
[86] K. Houben, S. Couet, M. Trekels, E. Menéndez, T. Peissker, J. W. Seo, M. Y. Hu, J. Y. Zhao, E. E. Alp, S. Roelants, B. Partoens, M. V. Milošević, F. M. Peeters, D. Bessas, S. A. Brown, A. Vantomme, K. Temst, M. J. V. Bael, *Phys. Rev. B* **2017**, *95*, 155413.
[87] K. Houben, J. K. Jochum, S. Couet, E. Menéndez, T. Picot, M. Y. Hu, J. Y. Zhao, E. E. Alp, A. Vantomme, K. Temst, M. J. Van Bael, *Sci. Rep.* **2020**, *10*, 5729.
[88] Q.-Y. Wang, Z. Li, W.-H. Zhang, Z.-C. Zhang, J.-S. Zhang, W. Li, H. Ding, Y.-B. Ou, P. Deng, K. Chang, J. Wen, C.-L. Song, K. He, J.-F. Jia, S.-H. Ji, Y.-Y. Wang, L.-L. Wang, X. Chen, X.-C. Ma, Q.-K. Xue, *Chin. Phys. Lett.* **2012**, *29*, 037402.
[89] S. Gerber, S.-L. Yang, D. Zhu, H. Soifer, J. A. Sobota, S. Rebec, J. J. Lee, T. Jia, B. Moritz, C. Jia, A. Gauthier, Y. Li, D. Leuenberger, Y. Zhang, L. Chaix, W. Li, H. Jang, J.-S. Lee, M. Yi, G. L. Dakovski, S. Song, J. M. Glownia, S. Nelson, K. W. Kim, Y.-D. Chuang, Z. Hussain, R. G. Moore, T. P. Devereaux, W.-S. Lee, P. S. Kirchmann, et al., *Science* **2017**, *357*, 71.
[90] M.-X. Wang, C. Liu, J.-P. Xu, F. Yang, L. Miao, M.-Y. Yao, C. L. Gao, C. Shen, X. Ma, X. Chen, Z.-A. Xu, Y. Liu, S.-C. Zhang, D. Qian, J.-F. Jia, Q.-K. Xue, *Science* **2012**, *338*, 1465.
[91] J. A. Hlevyack, S. Najafzadeh, M.-K. Lin, T. Hashimoto, T. Nagashima, A. Tsuzuki, A. Fukushima, C. Bareille, Y. Bai, P. Chen, R.-Y. Liu, Y. Li, D. Flötotto, J. Avila, J. N. Eckstein, S. Shin, K. Okazaki, T.-C. Chiang, *Phys. Rev. Lett.* **2020**, *124*, 236402.
[92] E. Moreno-Pineda, C. Godfrin, F. Balestro, W. Wernsdorfer, M. Ruben, *Chem. Soc. Rev.* **2018**, *47*, 501.
[93] A. Gaita-Ariño, F. Luis, S. Hill, E. Coronado, *Nat. Chem.* **2019**, *11*, 301.
[94] M. R. Wasielewski, M. D. E. Forbes, N. L. Frank, K. Kowalski, G. D. Scholes, J. Yuen-Zhou, M. A. Baldo, D. E. Freedman, R. H. Goldsmith, T. G. III, M. L. Kirk, J. K. McCusker, J. P. Ogilvie, D. A. Shultz, S. Stoll, K. B. Whaley, *Nat. Rev. Chem.* **2020**, *4*, 490.
[95] C. Bonizzoni, A. Ghirri, F. Santanni, M. Affronte, *npj Quantum Inf.* **2024**, *10*, 41.
[96] E. Garlatti, T. Guidi, S. Ansbro, P. Santini, G. Amoretti, J. Ollivier, H. Mutka, G. Timco, I. J. Vitorica-Yrezabal, G. F. S. Whitehead, R. E. P. Winpenny, S. Carretta, *Nat. Commun.* **2017**, *8*, 14543.
[97] S. Chicco, G. Allodi, A. Chiesa, E. Garlatti, C. D. Buch, P. Santini, R. De Renzi, S. Piligkos, S. Carretta, *J. Am. Chem. Soc.* **2024**, *146*, 1053.
[98] V. Corradini, A. Ghirri, E. Garlatti, R. Biagi, V. de Renzi, U. del Pennino, V. Bellini, S. Carretta, P. Santini, G. Timco, R. E. P. Winpenny, M. Affronte, *Adv. Func. Mater.* **2012**, *22*, 3706.
[99] M. Mannini, F. Pineider, C. Danieli, F. Totti, L. Sorace, P. Sainctavit, M.-A. Arrio, E. Otero, L. Joly, J. C. Cezar, A. Cornia, R. Sessoli, *Nature* **2010**, *468*, 417.

[100] J. Grunwald, J. Torres, A. Buchholz, C. Näther, L. Kämmerer, M. Gruber, S. Rohlf, S. Thakur, H. Wende, W. Plass, W. Kuch, F. Tuczek, *Chem. Sci.* **2023**, *14*, 7361.
[101] A. Hauser, in Spin Crossover in Transition Metal Compounds II, vol. *234*, *Topics in Current Chemistry* (Ed: P. Gütlich, H. A. Goodwin), Springer, Berlin, Heidelberg, **2004**.
[102] E. E. Garlatti, A. Albino, S. Chicco, V. H. A. Nguyen, F. Santanni, L. Paolasini, C. Mazzoli, R. Caciuffo, F. Totti, P. Santini, R. Sessoli, A. Lunghi, S. Carretta, *Nat. Commun.* **2023**, *14*, 1653.
[103] D. Ranieri, F. Santanni, A. Privitera, A. Albino, E. Salvadori, M. Chiesa, F. Totti, L. Sorace, R. Sessoli, *Chem. Sci.* **2022**, *14*, 61.
[104] C.-Z. Chang, C.-X. Liu, A. H. MacDonald, *Rev. Mod. Phys.* **2023**, *95*, 011002.
[105] K. von Klitzing, in *Encyclopedia of Condensed Matter Physics*, vol. *1*, (Ed: T. Chakraborty), 2nd ed. Elsevier, Amsterdam **2024**, pp. 1–8.
[106] C.-Z. Chang, J. Zhang, X. Feng, J. Shen, Z. Zhang, M. Guo, K. Li, Y. Ou, P. Wei, L.-L. Wang, Z.-Q. Ji, Y. Feng, S. Ji, X. Chen, J. Jia, X. Dai, Z. Fang, S.-C. Zhang, K. He, Y. Wang, L. Lu, X.-C. Ma, Q.-K. Xue, *Science* **2013**, *167*, 3406129.
[107] J. Sánchez-Barriga, O. J. Clark, O. Rader, in *Encyclopedia of Condensed Matter Physics*, 2nd ed., vol. *4*, (Ed: T. Chakraborty), Elsevier, Amsterdam, **2024**, pp. 334–369.
[108] G. Götz, K. M. Fijalkowski, E. Pesel, M. Hartl, S. Schreyeck, M. Winnerlein, S. Grauer, H. Scherer, K. Brunner, C. Gould, F. J. Ahlers, L. W. Molenkamp, *Appl. Phys. Lett.* **2018**, *112*, 072102.
[109] B. Jeckelmann, B. Jeanneret, *Rep. Prog. Phys.* **2001**, *64*, 1603.
[110] W. Poirier, F. Schopfer, *Eur. Phys. J. Spec. Top.* **2009**, *172*, 207.
[111] M. Kobayashi, I. Muneta, Y. Takeda, Y. Harada, A. Fujimori, J. Krempaský, T. Schmitt, S. Ohya, M. Tanaka, M. Oshima, V. N. Strocov, *Phys. Rev. B* **2014**, *89*, 205204.
[112] A. Tcakaev, V. B. Zabolotnyy, R. J. Green, T. R. F. Peixoto, F. Stier, M. Dettbarn, S. Schreyeck, M. Winnerlein, R. C. Vidal, S. Schatz, H. B. Vasili, M. Valvidares, K. Brunner, C. Gould, H. Bentmann, F. Reinert, L. W. Molenkamp, V. Hinkov, *Phys. Rev. B* **2020**, *101*, 045127.
[113] J. A. Krieger, C.-Z. Chang, M.-A. Husanu, D. Sostina, A. Ernst, M. M. Otrokov, T. Prokscha, T. Schmitt, A. Suter, M. G. Vergniory, E. V. Chulkov, J. S. Moodera, V. N. Strocov, Z. Salman, *Phys. Rev. B* **2017**, *96*, 184402.
[114] W. Li, M. Claassen, C.-Z. Chang, B. Moritz, T. Jia, C. Zhang, S. Rebec, J. J. Lee, M. Hashimoto, D.-H. Lu, R. G. Moore, J. S. Moodera, T. P. Devereaux, Z.-X. Shen, *Sci. Rep.* **2016**, *6*, 32732.
[115] E. D. L. Rienks, S. Wimmer, J. Sánchez-Barriga, O. Caha, P. S. Mandal, J. Růžička, A. Ney, H. Steiner, V. V. Volobuev, H. Groiss, M. Albu, G. Kothleitner, J. Michalička, S. A. Khan, J. Minár, H. Ebert, G. Bauer, F. Freyse, A. Varykhalov, O. Rader, G. Springholz, *Nature* **2019**, *576*, 423.
[116] Y. Deng, Y. Yu, M. Z. Shi, Z. Guo, Z. Xu, J. Wang, X. H. Chen, Y. Zhang, *Science* **2020**, *367*, 895.
[117] M. Mogi, R. Yoshimi, A. Tsukazaki, K. Yasuda, Y. Kozuka, K. S. Takahashi, M. Kawasaki, Y. Tokura, *Appl. Phys. Lett.* **2015**, *107*, 182401.
[118] A. L. Sharpe, E. J. Fox, A. W. Barnard, J. Finney, K. Watanabe, T. Taniguchi, M. Kastner, D. Goldhaber-Gordon, *Science* **2019**, *365*, 605.
[119] M. Serlin, C. Tschirhart, H. Polshyn, Y. Zhang, J. Zhu, K. Watanabe, T. Taniguchi, L. Balents, A. Young, *Science* **2020**, *367*, 900.
[120] G. Chen, A. L. Sharpe, E. J. Fox, Y.-H. Zhang, S. Wang, L. Jiang, B. Lyu, H. Li, K. Watanabe, T. Taniguchi, Z. Shi, T. Senthil, D. Goldhaber-Gordon, Y. Zhang, F. Wang, *Nature* **2020**, *579*, 56.
[121] T. Li, S. Jiang, B. Shen, Y. Zhang, L. Li, Z. Tao, T. Devakul, K. Watanabe, T. Taniguchi, L. Fu, J. Shan, K. F. Mak, *Nature* **2021**, *600*, 641.
[122] F. Jelezko, J. Wrachtrup, *Phys. Status Solidi A* **2006**, *203*, 3207.
[123] C. Zhang, F. Shagieva, M. Widmann, M. Kübler, V. Vorobyov, P. Kapitanova, E. Nenasheva, R. Corkill, O. Rörhle, K. Nakamura, H. Sumiya, S. Onoda, J. Isoya, J. Wrachtrup, *Phys. Rev. Applied* **2021**, *15*, 064075.
[124] G. Balasubramanian, I. Y. Chan, R. Kolesov, M. Al-Hmoud, J. Tisler, C. Shin, C. Kim, A. Wojcik, P. R. Hemmer, A. Krueger, T. Hanke, A. Leitenstorfer, R. Bratschitsch, F. Jelezko, J. Wrachtrup, *Nature* **2008**, *455*, 648.
[125] S. Sangtawesin, B. L. Dwyer, S. Srinivasan, J. J. Allred, L. V. H. Rodgers, K. De Greve, A. Stacey, N. Dontschuk, K. M. O'Donnell, D. Hu, D. A. Evans, C. Jaye, D. A. Fischer, M. L. Markham, D. J. Twitchen, H. Park, M. D. Lukin, N. P. de Leon, *Phys. Rev. X* **2019**, *9*, 031052.
[126] Z. Shpilman, I. Gouzman, T. K. Minton, L. Shen, A. Stacey, J. Orwa, S. Prawer, B. C. C. Cowie, A. Hoffman, *Diamond Relat. Mater.* **2014**, *45*, 20.
[127] M. W. Doherty, N. B. Manson, P. Delaney, F. Jelezko, J. Wrachtrup, L. C. L. Hollenberg, *Phys. Rep.* **2013**, *528*, 1.
[128] N. Manson, J. Harrison, *Diamond Relat. Mater.* **2005**, *14*, 1705.
[129] G. Wolfowicz, F. J. Heremans, C. P. Anderson, S. Kanai, H. Seo, A. Gali, G. Galli, D. D. Awschalom, *Nat. Rev. Mater.* **2021**, *6*, 906.
[130] S. J. Whiteley, F. J. Heremans, G. Wolfowicz, D. D. Awschalom, M. V. Holt, *Nat. Commun.* **2019**, *10*, 3386.
[131] A. L. Falk, P. V. Klimov, B. B. Buckley, V. Ivády, I. A. Abrikosov, G. Calusine, W. F. Koehl, A. Gáli, D. D. Awschalom, *Phys. Rev. Lett.* **2014**, *112*, 187601.
[132] N. Delegan, S. J. Whiteley, T. Zhou, S. L. Bayliss, M. Titze, E. Bielejec, M. V. Holt, D. D. Awschalom, F. J. Heremans, *Nanotechnology* **2023**, *34*, 385001.
[133] X. Ming, Y.-J. Zhang, X. Zhu, Q. Li, C. He, Y. Liu, T. Huang, G. Liu, B. Zheng, H. Yang, J. Sun, X. Xi, H.-H. Wen, *Nature* **2023**, *620*, 72.
[134] P. Bhattacharyya, W. Chen, X. Huang, S. Chatterjee, B. Huang, B. Kobrin, Y. Lyu, T. J. Smart, M. Block, E. Wang, Z. Wang, W. Wu, S. Hsieh, H. Ma, S. Mandyam, B. Chen, E. Davis, Z. M. Geballe, C. Zu, V. Struzhkin, R. Jeanloz, J. E. Moore, T. Cui, G. Galli, B. I. Halperin, C. R. Laumann, N. Y. Yao, *Nature* **2024**, *627*, 73.
[135] M. Wang, Y. Wang, Z. Liu, G. Xu, B. Yang, P. Yu, H. Sun, X. Ye, J. Zhou, A. F. Goncharov, Y. Wang, J. Du, *Nat. Commun.* **2024**, *15*, 8843.
[136] A. Hilberer, L. Toraille, C. Dailledouze, M.-P. Adam, L. Hanlon, G. Weck, M. Schmidt, P. Loubeyre, J.-F. Roch, *Phys. Rev. B* **2023**, *107*, L220102.
[137] N. Gisin, G. Ribordy, W. Tittel, H. Zbinden, *Rev. Mod. Phys.* **2002**, *74*, 145.
[138] A. Acín, N. Brunner, N. Gisin, S. Massar, S. Pironio, V. Scarani, *Phys. Rev. Lett.* **2007**, *98*, 230501.
[139] J. Kołodyński, A. Máttar, P. Skrzypczyk, E. Woodhead, D. Cavalcanti, K. Banaszek, A. Acín, *Quantum* **2020**, *4*, 260.
[140] T. Trong Tran, K. Bray, M. J. Ford, M. Toth, I. Aharonovich, *Nat. Nanotechnol.* **2016**, *11*, 37.
[141] G. Grosso, H. Moon, B. Lienhard, S. Ali, D. K. Efetov, M. M. Furchi, P. Jarillo-Herrero, M. J. Ford, I. Aharonovich, D. Englund, *Nat. Commun.* **2017**, *8*, 705.
[142] M. Kianinia, S. A. Tawfik, B. Regan, T. Trong Tran, M. J. Ford, I. Aharonovich, M. Toth, *ACS Photonics* **2017**, *4*, 768.
[143] M. Toth, I. Aharonovich, *Annu. Rev. Phys. Chem.* **2019**, *70*, 123.
[144] P. Kumar, F. Fabre, A. Durand, T. Clua-Provost, J. Li, J. H. Edgar, N. Rougemaille, J. Coraux, X. Marie, P. Renucci, C. Robert, I. Robert-Philip, B. Gil, G. Cassabois, A. Finco, V. Jacques, *Phys. Rev. Applied* **2022**, *18*, L061002.
[145] E. Paris, Y. Tseng, E. M. Pärschke, W. Zhang, M. H. Upton, A. Efimenko, K. Rolfs, D. E. McNally, L. Maurel, M. Naamneh, M. Caputo, V. N. Strocov, Z. Wang, D. Casa, C. W. Schneider, E. Pomjakushina, K. Wohlfeld, M. Radovic, T. Schmitt, *Proc. Natl. Acad. Sci. USA* **2020**, *117*, 24764.

[146] J. Pelliciari, E. Mejia, J. M. Woods, Y. Gu, J. Li, S. B. Chand, S. Fan, K. Watanabe, T. Taniguchi, V. Bisogni, G. Grosso, *Nat. Mater.* **2024**, *23*, 1230.
[147] K. F. Mak, J. Shan, *Nat. Photonics* **2016**, *10*, 216.
[148] H. Yuan, Z. Liu, G. Xu, B. Zhou, S. Wu, D. Dumcenco, K. Yan, Y. Zhang, S.-K. Mo, P. Dudin, V. Kandyba, M. Yablonskikh, A. Barinov, Z. Shen, S. Zhang, Y. Huang, X. Xu, Z. Hussain, H. Y. Hwang, Y. Cui, Y. Chen, *Nano Lett.* **2016**, *16*, 4738.
[149] M. Gehlmann, I. Aguilera, G. Bihlmayer, S. Nemšák, P. Nagler, P. Gospodarič, G. Zamborlini, M. Eschbach, V. Feyer, F. Kronast, E. Mlyńczak, T. Korn, L. Plucinski, C. Schüller, S. Blügel, C. M. Schneider, *Nano Lett.* **2017**, *17*, 5187.
[150] A. L. Exarhos, D. A. Hopper, R. R. Grote, A. Alkauskas, L. C. Bassett, *ACS Nano* **2017**, *11*, 3328.
[151] M. Nguyen, S. Kim, T. Trong Tran, Z.-Q. Xu, M. Kianinia, M. Toth, I. Aharonovich, *Nanoscale* **2018**, *10*, 2267.
[152] A. Hötger, J. Klein, K. Barthelmi, L. Sigl, F. Sigger, W. Männer, S. Gyger, M. Florian, M. Lorke, F. Jahnke, T. Taniguchi, K. Watanabe, K. D. Jöns, U. Wurstbauer, C. Kastl, K. Müller, J. J. Finley, A. W. Holleitner, *Nano Lett.* **2021**, *21*, 1040.
[153] A. E. Willner, K. Pang, H. Song, K. Zou, H. Zhou, *Appl. Phys. Rev.* **2021**, *8*, 041312.
[154] S. Sasaki, I. McNulty, *Phys. Rev. Lett.* **2008**, *100*, 124801.
[155] J. Bahrdt, K. Holldack, P. Kuske, R. Müller, M. Scheer, P. Schmid, *Phys. Rev. Lett.* **2013**, *111*, 034801.
[156] A. Mair, A. Vaziri, G. Weihs, A. Zeilinger, *Nature* **2001**, *412*, 313.
[157] M. Beye, S. Schreck, F. Sorgenfrei, C. Trabant, N. Pontius, C. Schüssler-Langeheine, W. Wurth, A. Föhlisch, *Nature* **2013**, *501*, 191.
[158] S. Shwartz, R. N. Coffee, J. M. Feldkamp, Y. Feng, J. B. Hastings, G. Y. Yin, S. E. Harris, *Phys. Rev. Lett.* **2012**, *109*, 013602.
[159] F. Bencivenga, R. Cucini, F. Capotondi, A. Battistoni, R. Mincigrucci, E. Giangrisostomi, A. Gessini, M. Manfredda, I. P. Nikolov, E. Pedersoli, E. Principi, C. Svetina, P. Parisse, F. Casolari, M. B. Danailov, M. Kiskinova, C. Masciovecchio, *Nature* **2015**, *520*, 205.
[160] S. Shwartz, M. Fuchs, J. B. Hastings, Y. Inubushi, T. Ishikawa, T. Katayama, D. A. Reis, T. Sato, K. Tono, M. Yabashi, S. Yudovich, S. E. Harris, *Phys. Rev. Lett.* **2014**, *112*, 163901.
[161] R. Röhlsberger, J. Evers, S. Shwartz, in *Synchrotron Light Sources and Free-Electron Lasers: Accelerator Physics, Instrumentation and Science Applications*, (Eds:. E. J. Jaeschke, S. Khan, J. R. Schneider, J. B. Hastings), Springer, Cham, **2020**, pp. 1399–1431.
[162] B. Seiferle, L. von der Wense, P. V. Bilous, I. Amersdorffer, C. Lemell, F. Libisch, S. Stellmer, T. Schumm, C. E. Düllmann, A. Pálffy, P. G. Thirolf, *Nature* **2019**, *573*, 243.
[163] P. M. Eisenberger, S. L. McCall, *Phys. Rev. Lett.* **1971**, *26*, 684.
[164] B. W. Adams, C. Buth, S. M. Cavaletto, J. Evers, Z. Harman, C. H. Keitel, A. Pálffy, A. Picón, R. Röhlsberger, Y. Rostovtsev, K. Tamasaku, *Nat. Photonics* **2013**, *60*, 2.
[165] A. F. Abouraddy, P. R. Stone, A. V. Sergienko, B. E. A. Saleh, M. C. Teich, *Phys. Rev. Lett.* **2004**, *93*, 213903.
[166] A. Schori, D. Borodin, K. Tamasaku, S. Shwartz, *Phys. Rev. A* **2018**, *97*, 063804.
[167] S. Sofer, E. Strizhevsky, A. Schori, K. Tamasaku, S. Shwartz, *Phys. Rev. X* **2019**, *9*, 031033.
[168] A. Nazarkin, S. Podorov, I. Uschmann, E. Förster, R. Sauerbrey, *Phys. Rev. A* **2003**, *67*, 041804.
[169] T. E. Glover, D. M. Fritz, M. Cammarata, T. K. Allison, S. Coh, J. M. Feldkamp, H. Lemke, D. Zhu, Y. Feng, R. N. Coffee, M. Fuchs, S. Ghimire, J. Chen, S. Shwartz, D. A. Reis, S. E. Harris, J. B. Hastings, *Nature* **2012**, *488*, 603.
[170] A. Di Meglio, K. Jansen, I. Tavernelli, C. Alexandrou, S. Arunachalam, C. W. Bauer, K. Borras, S. Carrazza, A. Crippa, V. Croft, R. de Putter, A. Delgado, V. Dunjko, D. J. Egger, E. Fernández-Combarro, E. Fuchs, L. Funcke, D. González-Cuadra, M. Grossi, J. C. Halimeh, Z. Holmes, S. Kühn, D. Lacroix, R. Lewis, D. Lucchesi, M. L. Martinez, F. Meloni, A. Mezzacapo, S. Montangero, L. Nagano, et al., *PRX Quantum* **2024**, *5*, 037001.
[171] C. W. Bauer, Z. Davoudi, A. B. Balantekin, T. Bhattacharya, M. Carena, W. A. D. Jong, P. Draper, A. El-Khadra, N. Gemelke, M. Hanada, D. Kharzeev, *PRX Quantum* **2023**, *4*, 027001.
[172] K. Dremel, D. Prjamkov, M. Firsching, M. Weule, T. Lang, A. Papadaki, S. Kasperl, M. Blaimer, T. O. Fuchs, *IEEE Trans. Quantum Eng.* **2025**, *6*, 3100810.
[173] K. Blekos, D. Brand, A. Ceschini, C. H. Chou, R. H. Li, K. Pandya, A. Summer, *Phys. Rep.* **2024**, *1068*, 1.
[174] L. K. Grover, in *Proceedings of the twenty-eighth annual ACM symposium on Theory of Computing.*, ACM, New York **1996**, p. 212.
[175] P. W. Shor, In *Proceedings 35th annual symposium on foundations of computer science*. IEEE, Santa Fe, **1994**, p. 124.
[176] W. Guan, G. Perdue, A. Pesah, M. Schuld, K. Terashi, S. Vallecorsa, J. R. Vlimant, *Mach. Learn.: Sci. Technol.* **2021**, *2*, 011003.
[177] S. L. Wu, S. Sun, W. Guan, C. Zhou, J. Chan, C. L. Cheng, T. C. Wei, *Phys. Rev. Res.* **2021**, *3*, 033221.
[178] S. C. Leemann, S. Liu, A. Hexemer, M. A. Marcus, C. N. Melton, H. Nishimura, C. Sun, *Phys. Rev. Lett.* **2019**, *123*, 194801.
[179] Z. Chen, N. Andrejevic, N. C. Drucker, T. Nguyen, R. P. Xian, T. Smidt, M. Li, *Chem. Phys. Rev.* **2021**, *2*, 031301.
[180] C. D. Rankine, T. J. Penfold, *J. Phys. Chem. A* **2021**, *125*, 4276.
[181] V. Stanev, K. Choudhary, A. G. Kusne, *Commun. Mater.* **2021**, *2*, 105.
[182] G. Kourousias, F. Billè, F. Guzzi, M. Ippoliti, V. Bonanni, A. Gianoncelli, *PLoS One* **2023**, *18*, e0285057.
[183] A. Barbour, S. Campbell, T. Caswell, M. Fukuto, M. Hanwell, A. Kiss, T. Konstantinova, R. Laasch, P. Maffettone, B. Ravel, D. Olds, *Synchrotron Radiat. News* **2022**, *35*, 44.
[184] S. Birnsteinova, D. E. Ferreira de Lima, E. Sobolev, H. J. Kirkwood, V. Bellucci, R. J. Bean, C. Kim, J. C. P. Koliyadu, T. Sato, F. Dall'Antonia, E. M. Asimakopoulou, Z. Yao, K. Buakor, Y. Zhang, A. Meents, H. N. Chapman, A. P. Mancuso, P. Villanueva-Perez, P. Vagovič, *J. Synchrotron Radiat.* **2023**, *30*, 1030.
[185] Y. Sun, S. Brockhauser, P. Hegedűs, C. Plückthun, L. Gelisio, D. E. Ferreira de Lima, *Sci. Rep.* **2023**, *13*, 9370.
[186] D. E. Ferreira de Lima, A. Davtyan, J. Laksman, N. Gerasimova, T. Maltezopoulos, J. Liu, P. Schmidt, T. Michelat, T. Mazza, M. Meyer, J. Grünert, L. Gelisio, *Commun. Phys.* **2024**, *7*, 400.
[187] S. L. Wu, J. Chan, A. Cheng, W. Guan, S. J. Sun, R. Zhang, D. Walkerg, in *Proceedings of Science, EPS-HEP2021*. **2022**, p. 842.
[188] A. D. King, A. Nocera, M. M. Rams, J. Dziarmaga, R. Wiersema, W. Bernoudy, M. H. Amin, *Science* **2025**, *388*, 199.
[189] I. T. Rosen, S. Muschinske, C. N. Barrett, *Nat. Phys.* **2024**, *20*, 1881.
[190] G. Mussardo, A. Stampiggi, A. Trombettoni, *EPJ Quantum Technol.* **2024**, *11*, 65.
[191] E. T. Mannila, P. Samuelsson, S. Simbierowicz, J. T. Peltonen, V. Vesterinen, L. Grönberg, J. Hassel, V. F. Maisi, J. P. Pekola, *Nat. Phys.* **2022**, *18*, 145.
[192] D. Buterakos, S. Das Sarma, *PRX Quantum* **2021**, *2*, 040358.
[193] J. Noborisaka, T. Hayashi, A. Fujiwara, K. Nishiguchi, *J. Appl. Phys.* **2024**, *135*, 204302.
[194] L.-T. Tseng, P. Karadan, D. Kazazis, P. C. Constantinou, T. J. Z. Stock, N. J. Curson, S. R. Schofield, M. Muntwiler, G. Aeppli, Y. Ekinci, *Sci. Adv.* **2023**, *9*, eadf5997.
[195] M. Gilbert, *Commun. Phys.* **2021**, *4*, 70.
[196] Z. Dai, L. Liu, Z. Zhang, *Adv. Mater.* **2019**, *31*, 1805417.
[197] M. Prabhu, C. Errando-Herranz, L. D. Santis, I. Christen, C. Chen, C. Gerlach, D. Englund, *Nat. Commun.* **2023**, *14*, 2380.
[198] P. Udvarhelyi, B. Somogyi, G. Thiering, A. Gali, *Phys. Rev. Lett.* **2021**, *127*, 196402.

[199] K. Witte, A. Späth, S. Finizio, C. Donnelly, B. Watts, B. Sarafimov, M. Odstrcil, M. Guizar-Sicairos, M. Holler, R. H. Fink, J. Raabe, *Nano Lett.* **2020**, *20*, 1305.
[200] K.-J. Kim, Y. Shvyd'ko, S. Reiche, *Phys. Rev. Lett.* **2008**, *100*, 244802.
[201] Z. Huang, R. D. Ruth, *Phys. Rev. Lett.* **2006**, *96*, 144801.
[202] J. Feldhaus, E. Saldin, J. Schneider, E. Schneidmiller, M. Yurkov, *Opt. Commun.* **1997**, *140*, 341.
[203] J. Amann, W. Berg, V. Blank, F.-J. Decker, Y. Ding, P. Emma, Y. Feng, J. Frisch, D. Fritz, J. Hastings, Z. Huang, J. Krzywinski, R. Lindberg, H. Loos, A. Lutman, H.-D. Nuhn, D. Ratner, J. Rzepiela, D. Shu, Y. Shvyd'ko, S. Spampinati, S. Stoupin, S. Terentyev, E. Trakhtenberg, D. Walz, J. Welch, J. Wu, A. Zholents, D. Zhu, *Nat. Photonics* **2012**, *6*, 693.
[204] S. Liu, C. Grech, M. Guetg, *Nat. Photonics* **2023**, *17*, 984.
[205] Y. Shvyd'ko, R. Röhlsberger, O. Kocharovskaya, J. Evers, G. A. Geloni, P. Liu, D. Shu, A. Miceli, B. Stone, W. Hippler, B. Marx-Glowna, I. Uschmann, R. Loetzsch, O. Leupold, H.-C. Wille, I. Sergeev, M. Gerharz, X. Zhang, C. Grech, M. Guetg, V. Kocharyan, N. Kujala, S. Liu, W. Qin, A. Zozulya, J. Hallmann, U. Boesenberg, W. Jo, J. Möller, A. Rodriguez-Fernandez, et al., *Nature* **2023**, *622*, 471.